Department of Biotechnology and Chemical Technology

Studies on polymeric composites with Ni-Mn-Ga alloys and carbon nanotubes

Mika Lahelin

Aalto University

DOCTORAL DISSERTATIONS

Aalto University publication series
DOCTORAL DISSERTATIONS 126/2011

Studies on polymeric composites with Ni-Mn-Ga alloys and carbon nanotubes

Mika Lahelin

Doctoral dissertation for the degree of Doctor of Science in Technology to be presented with due permission of the School of Chemical Technology for public examination and debate in Auditorium KE2 (Komppa Auditorium) at the Aalto University School of Chemical Technology (Espoo, Finland) on the 9th of December, 2011, at 12 noon.

Aalto University
School of Chemical Technology
Department of Biotechnology and Chemical Technology
Polymer Technology

Supervisor
Professor Jukka Seppälä

Instructor
Professor Jukka Seppälä

Preliminary examiners
Professor Ulf Gedde, Royal Institute of Technology, Sweden
Doctor Antti Helminen, Premix Oy, Finland

Opponent
Professor Jyrki Vuorinen, Tampere University of Technology, Finland

Aalto University publication series
DOCTORAL DISSERTATIONS 126/2011

ISBN 978-952-60-4387-6 (printed)
ISBN 978-952-60-4388-3 (pdf)
ISSN-L 1799-4934
ISSN 1799-4934 (printed)
ISSN 1799-4942 (pdf)

Unigrafia Oy
Helsinki 2011

Finland

The dissertation can be read at http://lib.tkk.fi/Diss/

Publication orders (printed book):
Aalto University, Department of Biotechnology and Chemical Technology

NORDIC ECOLABEL
441 697
Printed matter

Author
Mika Lahelin

Name of the doctoral dissertation
Studies on polymeric composites with Ni-Mn-Ga alloys and carbon nanotubes

Publisher School of Chemical Technology

Unit Department of Biotechnology and Chemical Technology

Series Aalto University publication series DOCTORAL DISSERTATIONS 126/2011

Field of research Polymer Technology

Manuscript submitted 10 August 2011 **Manuscript revised** 18 October 2011

Date of the defence 9 December 2011 **Language** English

☐ **Monograph** ☒ **Article dissertation (summary + original articles)**

Abstract

In the first part of the study, the temperature and stress dependencies on the damping of bulk Ni-Mn-Ga alloys were studied. The measurements showed a significant decrease in the storage modulus values in martensite region for all alloys with an increasing temperature. The loss modulus values were almost constant in the martensite phase, decreasing to ~ zero at the martensite to austenite transformation. The damping of bulk Ni-Mn-Ga decreased sharply at the transformation temperature. The stress dependency on the damping was measured for a non-modulated Ni-Mn-Ga alloy, showing a certain level of stress, twinning stress, which must be overcome before the twins in an Ni-Mn-Ga alloy can begin to move, and the damping due to the twin movement can be activated.

Polymer composites were manufactured using Ni-Mn-Ga as powder, ribbons, and thin bulk. The adhesion between Ni-Mn-Ga and the polymers was studied for epoxies, silicones, and polyurethanes. Epoxies with different mechanical strength levels were tested, the epoxies with strength levels comparable to the used Ni-Mn-Ga showed improvements in passive damping. A magnetic circuit was constructed for dynamic mechanical analysis, and an improvement in damping was found with an external magnetic field and with Ni-Mn-Ga powder orientation in epoxy matrix.

In the second part of the study, methyl methacrylate was in situ polymerized in the presence of carbon nanotubes. Both the low molecular weight anionic surfactants and amphiphilic copolymers with a significantly higher molecular weight were used as dispersing agents. Both types of surfactants were able to effectively disperse the multi-walled carbon nanotubes into the polymer matrix. Carbon nanotubes, surfactants, and initiators all had an influence on polymerization and on the molecular weight of the resulting polymer. The modulus values of the composites were improved, and the stress at break values improved or remained stable up to high carbon nanotube loading (6 wt.%), which further confirmed a good dispersion of carbon nanotubes. The electrical and thermal conductivities were both improved by the addition of carbon nanotubes. The composites were also tested as masterbatches. The electrical percolation threshold was lower with the masterbatch-approach than with the direct extrusion of carbon nanotubes and poly(methyl methacrylate). The viscosities of the melts had a significant influence on the extrusion and thus percolation threshold.

Keywords composite, Ni-Mn-Ga, damping, carbon nanotubes, dispersion, DMA

ISBN (printed) 978-952-60-4387-6 **ISBN (pdf)** 978-952-60-4388-3

ISSN-L 1799-4934 **ISSN (printed)** 1799-4934 **ISSN (pdf)** 1799-4942

Location of publisher Espoo **Location of printing** Helsinki **Year** 2011

Pages 134 **The dissertation can be read at** http://lib.tkk.fi/Diss/

Tekijä
Mika Lahelin

Väitöskirjan nimi
Tutkimuksia Ni-Mn-Ga -metalliseoksiin ja hiilen nanoputkiin pohjautuvista polymeerikomposiiteista

Julkaisija Kemian tekniikan korkeakoulu

Yksikkö Biotekniikan ja kemian tekniikan laitos

Sarja Aalto University publication series DOCTORAL DISSERTATIONS 126/2011

Tutkimusala Polymeeriteknologia

Käsikirjoituksen pvm 10.08.2011 **Korjatun käsikirjoituksen pvm** 18.10.2011

Väitöspäivä 09.12.2011 **Kieli** Englanti

☐ **Monografia** ☒ **Yhdistelmäväitöskirja (yhteenveto-osa + erillisartikkelit)**

Tiivistelmä

Aluksi tutkittiin Ni-Mn-Ga -metalliseosten vaimennuksen lämpötila- ja jännitysriippuvuutta. Mittaukset osoittivat varastomoduulin laskevan merkittävästi martensiittisella alueella lämpötilan noustessa. Häviömoduulin arvo pysyi lähes vakiona pudoten sitten voimakkaasti martensiittitilan muuttuessa austeniitiksi. Vastaavasti Ni-Mn-Ga -seosten vaimennuskyky aleni voimakkaasti muutoslämpötilassa. Vaimennuksen jännitysriippuvuutta testattiin moduloimattomalla Ni-Mn-Ga -metalliseoksella. Mittaukset osoittivat, että tehokas vaimennus vaati tietyn kuormitustason (twinning stress) ylittämistä, jotta kaksoset alkoivat liikkua.

Tutkimusta jatkettiin valmistamalla polymeerikomposiitteja, joissa käytettiin Ni-Mn-Ga -metalliseoksia pulverina, nauhoina ja ohutlevyinä. Testattiin Ni-Mn-Ga:n ja polymeerien, kuten epoksien, silikonien ja polyuretaanien, välistä adheesiota. Polymeeri/Ni-Mn-Ga -komposiiteista korkeimmat passiiviset vaimennukset saavutettiin epokseilla, joiden mekaaniset ominaisuudet lähinnä vastasivat käytetyn Ni-Mn-Ga -seoksen mekaanisia ominaisuuksia. Dynaamiselle mekaaniselle testauslaitteelle rakennettiin magneettipiiri, jotta voitiin testata aktiivista vaimennusta. Sekä ulkoisen magneettikentän että Ni-Mn-Ga -pulverin orientoinnin komposiitissa todettiin nostavan vaimennusta.

Tutkimuksen jälkimmäisessä osassa metyylimetakrylaattia in situ -polymeroitiin hiilen nanoputkien läsnäollessa. Dispergointiaineina käytettiin sekä alhaisen moolimassan anionisia pinta-aktiivisia aineita että merkittävästi korkeamman moolimassan amfifiilisia kopolymeereja. Molemmat ryhmät dispergoivat moniseinäisiä nanoputkia tehokkaasti polymeerimatriisiin. Hiilen nanoputkilla, surfaktantilla ja initiaattorilla oli merkittävästi vaikutusta polymerointiin ja muodostuvan polymeerin moolimassaan. Komposiittien moduulit nousivat ja murtokuormitukset pysyivät vakaina tai paranivat aina 6 p-% nanoputkipitoisuuteen asti, mikä osaltaan vahvisti käsitystä hyvästä dispersiosta. Sähkön- ja lämmönjohtavuudet paranivat hiilen nanoputkien lisäyksellä. Lopuksi komposiitteja testattiin masterbatsina. Sähkönjohtavuuden perkolaatioraja oli matalampi masterbatsia käytettäessä kuin suoraan hiilen nanoputkia ja polymetyylimetakrylaattia seostettaessa. Sulaviskositeetilla havaittiin olevan huomattavaa merkitystä komposiittien sulatyöstössä ja perkolaatiossa.

Avainsanat komposiitti, Ni-Mn-Ga, vaimennus, hiilen nanoputket, dispersio, DMA

ISBN (painettu) 978-952-60-4387-6 **ISBN (pdf)** 978-952-60-4388-3

ISSN-L 1799-4934 **ISSN (painettu)** 1799-4934 **ISSN (pdf)** 1799-4942

Julkaisupaikka Espoo **Painopaikka** Helsinki **Vuosi** 2011

Sivumäärä 134 **Luettavissa verkossa osoitteessa** http://lib.tkk.fi/Diss/

Preface

This work was carried out in the Polymer Technology Research Group at Aalto University School of Chemical Technology between 2005 and 2011 (Helsinki University of Technology until January 2010). Financial support from TEKES (the Finnish Funding Agency for Technology and Innovation), and the Graduate School of the Processing of Polymers and Polymer-based Multimaterials (POPROK) is deeply appreciated.

I wish to express my gratitude to my supervisor, Professor Jukka Seppälä, for the opportunity to work in his research group. I am also grateful for Professor Simo-Pekka Hannula for an opportunity to co-work with his research group. Dr. Barbro Löfgren is thanked for the guidance and support.

I want to thank Ilkka Aaltio, Dr. Outi Söderberg, Minna Annala, Arja Vesterinen, and all the people involved in the TEKES projects DEMSMAC I/II and JOPO for fruitful co-operation. Thanks are extended to all co-authors for their valuable contribution and comments. The students and trainees who participated in this work are also thanked. Mary Metzler and Darin Nolan are thanked for revising the language of the publications and the thesis. All colleagues and personnel of the research group are thanked for pleasant working atmosphere.

Finally, my dearest thanks for my parents, Riitta† and Keijo, for their support and encouragement throughout the years.

Espoo, November 2011

Mika Lahelin

CONTENTS

LIST OF PUBLICATIONS

ABBREVIATIONS AND SYMBOLS

LIST OF PUBLICATIONS

This thesis consists of an overview and of the following six publications, which are referred to in the text by their Roman numerals.

I Aaltio, I., Lahelin, M., Söderberg, O., Heczko, O., Löfgren, B., Ge, Y., Seppälä, J., Hannula, S.-P., Temperature dependence of the damping properties of Ni-Mn-Ga alloys, *Mater. Sci. Eng. A* **481-482** (2008) 314-317.

II Aaltio, I., Mohanchandra, K.P., Heczko, O., Lahelin, M., Ge, Y., Carman, G.P., Söderberg, O., Löfgren, B., Seppälä, J., Hannula, S.-P., Temperature dependence of mechanical damping in Ni-Mn-Ga austenite and non-modulated martensite, *Scripta Mater.* **59** (2008) 550-553.

III Lahelin, M., Aaltio, I., Heczko, O., Söderberg, O., Ge, Y., Löfgren, B., Hannula, S.-P., Seppälä, J., DMA testing of Ni-Mn-Ga/polymer composites, *Compos. Part A* **40** (2009) 125-129.

IV Lahelin, M., Annala, M., Nykänen, A., Ruokolainen, J., Seppälä, J., In situ polymerized nanocomposites: polystyrene/CNT and poly(methyl methacrylate)/CNT composites, *Compos. Sci. Tech.* **71** (2011) 900-907.

V Lahelin, M., Vesterinen, A., Nykänen, A., Ruokolainen, J., Seppälä, J., In situ polymerization of methyl methacrylate/multi-walled carbon nanotube composites using cationic stearyl methacrylate copolymers as dispersants, *Eur. Polym. J.* **47** (2011) 873-881.

VI Annala, M., Lahelin, M., Seppälä, J., Utilization of PMMA-CNT and PS-CNT in situ polymerized composites as masterbatches for melt mixing. *Submitted.*

The author's contribution to the appended publications

I Mika Lahelin planned and carried out the dynamical mechanical analysis testing, and co-wrote the manuscript with the co-authors.

II Mika Lahelin assisted in planning and analyzing the dynamical mechanical analysis experiments and results, and assisted in the preparation of the manuscript.

III Mika Lahelin prepared the composites and carried out the characterizations (excluding electron microscopy), and wrote the manuscript with the assistance of the co-authors.

IV Mika Lahelin planned and carried out the polymerizations and characterizations (excluding electron microscopy) of poly(methyl methacrylate) based composites, and wrote the manuscript with the assistance of the co-authors.

V Mika Lahelin planned and carried out the polymerizations and characterizations (excluding electron microscopy) of composites, and wrote the manuscript with the assistance of the co-authors.

VI Mika Lahelin planned and carried out the polymerization and characterization of poly(methyl methacrylate) polymers, and assisted in the preparation of the manuscript.

ABBREVIATIONS AND SYMBOLS

10M / 5M	5-layered modulated martensite
14M / 7M	7-layered modulated martensite
2M / NM	non-modulated martensite
AIBN	azobisisobutyronitrile
A_f	austenite transformation finish temperature [K]
A_s	austenite transformation start temperature [K]
CNT	carbon nanotube
CVD	chemical vapor deposition
DBSA	sodium dodecyl benzene sulfate
DMA	dynamic mechanical analysis
DSC	differential scanning calorimetry
DWCNT	double-walled carbon nanotube
E'	storage modulus [Pa]
E''	loss modulus [Pa]
KPS	potassium peroxodisulfate
M_f	martensite transformation finish temperature [K]
MMA	methyl methacrylate
M_n	number average molecular weight [g/mol]
M_s	martensite transformation start temperature [K]
M_w	weight average molecular weight [g/mol]
MSM	magnetic shape memory
MSME	magnetic shape memory effect
MWCNT	multi-walled carbon nanotube
PD	polydispersity
PMMA	poly(methyl methacrylate)
SDS	sodium dodecyl sulfate
SEC	size exclusion chromatography
SEM	scanning electron microscopy
SMA	shape memory alloy
SMA	stearyl methacrylate
SME	shape memory effect
SWCNT	single-walled carbon nanotube
tan δ	damping factor (E''/E')
TEM	transmission electron microscopy
T_c	Curie temperature [K]
T_g	glass transition temperature [K or °C]

1. INTRODUCTION

1.1 A general background on polymeric composites

Polymers are low-density materials, easy to mould into a required shape, and they have a high damping capability, all properties which make them an excellent choice for many applications. Polymers are also relatively inexpensive materials. On the negative side, their mechanical properties are limited when compared to metals or ceramics. Special engineering polymers exist, which have better properties than mass-scale polymers such as polyolefins, polystyrene or poly(methyl methacrylate), but they are more expensive. Common limitations with polymers are also their electrical and thermal conductivities, which are generally low, expect for some special conductive polymers, and their low operating temperature. To overcome some of these material limitations, composites of polymer combined, with fillers, can be used. With polymeric composites, the polymer acts as a matrix surrounding and supporting the filler, which provides improvements in, for example, mechanical or conductive properties.

Traditional polymeric composites, such as carbon-fibre based polyolefins, can have a high amount of fillers, up to tens of wt.%. When a specific property is improved by a filler, the filler might have a negative influence on other composite properties. For example, a high amount of carbon-black for electrical conductivity often has a negative effect on mechanical properties. Nanoparticles are a group of structures, where at least one dimension of the particle is required to be on a nanometer scale; usually defined as under 100 nanometers. Nanoparticles can have different shapes, such as spherical, tube-like, plate-like or they can be cluster-like. Nanoparticles are an interesting group of materials, as their small size can provide them with properties, which can radically differentiate from the bulk properties of the same material. A nanosize filler has a significantly larger specific surface area than a “traditional” filler, leading to an enhanced interaction with a polymer matrix, in the case of polymeric composites. Compared to traditional fillers, if a significantly lower amount of nanoscale fillers can provide the same enhancement for a polymer matrix, the negative effects of the filler can be lowered, or even completely eliminated.[1-2]

The dispersion of fillers into the polymer matrix and the interaction between the filler and the polymer are critical parameters for the composite. Nanoscale fillers are especially difficult to disperse as they have a strong tendency to re-aggregate, due to their strong Van der Waals forces. A uniform dispersion of fillers into the matrix is often desired, and especially with non-spherical fillers, orientating the fillers within the matrix can be beneficial for composite properties such as mechanical strength.[3] A magnetic or electrical field can be used to orient certain fillers in a matrix.

1.2 Shape memory alloys (SMAs) and their polymeric composites

Shape memory alloys (SMAs) are metallic compounds, such as Fe-Pd, Co-Ni-Ga, Ni-Mn-Al, and Ni-Mn-Ga. At a high temperature, they have a cubic crystal structure, which is then transformed by a martensitic reaction into another crystal structure, like tetragonal, orthorhombic, hexagonal, etc. at a lower temperature. A martensitic transformation can enable a significant shape change, but as the crystal structure change is dependent on the temperature, utilizing the shape memory effect (SME) requires cooling and heating cycles. Magnetic shape memory (MSM) alloys are a group of SMA materials, which can achieve high actuation rates (even up to 100 Hz), shape changes up to several percent at an ambient temperature, besides the normal SME. The MSM effect is based on an applied magnetic field (usually ~ 1 T). The requirement for the magnetic field to be able to trigger the shape change is magnetic ordering, so the alloy is required to be ferromagnetic or ferri/antiferromagnetic. The intensity of the MSM effect (or MSME) is dependent on crystal lattice deformation, and can be up to 10 % (Ni-Mn-Ga). There are several other shape change types induced by a magnetic field, such as conventional magnetostriction (MS), where the deformation is caused by a magnetization rotation relative to a crystal lattice, magnetic field assisted superelasticity (MFAS), and giant magnetocaloric effect (GMCE), but they are not explained in detail here. It is usual for SMA material to have several possible magnetic field induced effects, in addition to the SME with a temperature, which can be used to design so-called smart materials, responding to different stimuli.[4-8]

1.2.1 Ni-Mn-Ga alloys

Although a number of metallic alloys with different shape change profiles do exist, the most successful by far has been Ni-Mn-Ga. Ni-Mn-Ga has an extraordinary large shape change, up to 10 percent with a relatively low

applied magnetic field. Ni-Mn-Ga alloys can be divided into three main classes. 10M (or 5M in some older publications) has a tetragonal martensite structure with a maximum 6 percent shape change under a magnetic field. 14M (or 7M) has an orthorhombic martensite structure with up to 10 percent shape change under a magnetic field. The third type of Ni-Mn-Ga are 2M (or NM) alloys, which do not show any significant magnetic shape change under a magnetic field. Both the 10M and 14M variants have an MSME above room temperature (a maximum temperature of approximately 333K for 10M and 368K for 14M), which, although limiting, is still reasonably suitable for applications.[9-11] All three of the Ni-Mn-Ga variants have the usual SME effect present, which can be triggered by temperature change. [12-13] The MSM effect under a magnetic strain is based on highly mobile twin boundaries on Ni-Mn-Ga, making it possible for the magnetic stress, created by the magnetic field, to be larger than the twinning stress, which is working against the reorientation of twins. As a large external magnetic field is not preferable, the twinning stress should be low. With a low twinning stress, the increasing magnetic field will reorientate the twins until a certain saturation level is reached and the whole twinning structure is (preferably) changed into a single-variant state. A further increase of the magnetic field does not result in a larger magnetic induced shape change. The principle of a twin boundary movement under a magnetic field is shown in Fig. 1. The shape change occurs via a twin boundary motion, so that variants having the short c-axis, which is the easy axis of magnetization (10M and 14M), along the magnetic field, become the dominant variant. The material will contract in the direction of the magnetic field. If the magnetic field is removed, and no external force is applied, the shape change will remain. However, if some secondary variants still exist after the magnetic field has been applied, some recovery might occur when the magnetic field has been removed.[4-5, 8, 14-19]

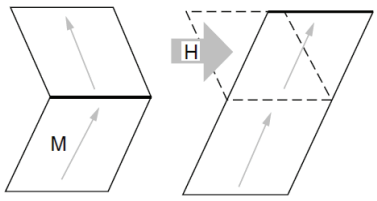

Fig. 1. Magnetic field-induced twin boundary motion.[4] Reprinted with permission from John Wiley & Sons, Inc.

Besides a magnetic field, the applied external stress can also be used with Ni-Mn-Ga. If the applied external stress exceeds the twinning stress, the twin boundary movement can be activated. Applied external stress can bring the Ni-Mn-Ga multivariant structure into a single-variant structure, or after the external magnetic field has been removed and the Ni-Mn-Ga is in a single-variant state, an external stress can be applied to return the material into the initial state. By combining both the external magnetic field and the external stress, interesting possibilities, for example, for actuator control, can be realized. The external stress can also be used to "train" the Ni-Mn-Ga, which makes it possible to affect the twinning stress to some degree. The level of internal twinning stress depends on many factors on crystals such as grain boundaries, crystal microcracks, variant inhomogeneities, and different impurities in the crystal. Besides the crystal structure, the surface treatment of crystals has also been shown to have a significant influence on twinning stress. Polishing can remove stresses that have built up during the cutting procedure of the crystals; significant stresses may also build up during the milling procedure, when producing particles of SMA materials.[20-21]

Although the Ni-Mn-Ga has excellent shape change properties, these properties have only been fully realized with single crystals. Ni-Mn-Ga, like all other metal alloys, can either be a single crystal or polycrystal material; some also use the term, oligocrystal material, which is a structure with "small" single crystals. A single crystal has the same crystal structure over the entire sample. With polycrystals, there are always grain boundaries and the variants cannot change freely over the whole sample, under the external magnetic field. This means that the polycrystals only have a limited MSM effect when compared to single crystal material. As a consequence, the polycrystal Ni-Mn-Ga is relatively brittle material, which tends to break when placed under long-term external stress. There are methods such as hot rolling or controlled porosity, which, combined with extensive training, can be used to lower the twinning stress of polycrystalline material, and to enable a low level MSM effect. The maximum shape change under an external magnetic field for polycrystals, however, is lower, when compared to single crystals. Overall, as the manufacturing of a single crystal Ni-Mn-Ga alloy is rather difficult and time consuming, and even a very small variation in the Ni-Mn-Ga composition can have a large effect on the crystal structure of the alloy, the maximum shape change is usually lower than the theoretical maximum value.[4-5, 8, 23-24]

1.2.2 Applications for shape changing materials

There are interesting applications for Ni-Mn-Ga with shape memory effects, most developments have been made on actuators. Bulk MSM actuators can produce an axial or bending motion, or force, when the MSM element is under an external magnetic field. The basic actuator design is simple: a bulk MSM element with an electromagnetic circuit, combined with a returning spring. This kind of design can usually produce up to a 4 % strain with a normal AC actuation. MSM based actuators can work at high frequencies, however, at frequencies over 100 Hz, the strain usually starts to decrease.[4,6] An important design factor of a bulk Ni-Mn-Ga for actuator use is the MSM behaviour at high cycling and the long-term durability. At high cycling, locked twin boundaries might appear which tends to decrease the maximum strain. Also, if the Ni-Mn-Ga material contains errors or microcracks, these tend to grow as the number of cycling increases; this may eventually lead to a failure of the actuator. Fatigue test studies have been carried out by few research groups and the results have varied significantly.[4] Another interesting application for a Ni-Mn-Ga MSM effect is energy harvesting, which is the reverse application for an actuator. Mechanical energy affects the bulk component, which changes the magnetification of the MSM element, which in turn results in a voltage peak.[25] By properly designing the material properties, element geometries, magnetic field, and the switching speed, the voltage generation can be regulated. Both actuator and energy harvesting design are promising application targets for Ni-Mn-Ga alloys, but both are still in the development stage and not ready for large scale use.[4-8] As applications indicate, Ni-Mn-Ga alloys can effectively absorb energy, indicating that they are suitable for vibration damping. Vibration damping can be either passive, semi-active or active, the latter being controlled by some external force, usually a magnetic field. As most polymers have good damping properties, Ni-Mn-Ga/polymer composites could be very promising candidates for controlled damping (via an external magnetic field). [26-27]

1.2.3 Composites based on Ni-Mn-Ga alloys

The single crystal Ni-Mn-Ga alloy is expensive to produce, and limited in size and form due to production restrictions. By combining a polymer matrix with Ni-Mn-Ga, the price of the product can be lower, as the polymers are usually much cheaper than the Ni-Mn-Ga alloy. The Ni-Mn-Ga alloy in polymer-based composites has been usually in particle form, as

the particles can be easily produced via different methods, such as spark erosion, the crushing of ingots, or the crushing of fibres or ribbons. The use of polymer-based composites will also make it possible to design the product size and form freely, which is not the case with single crystal bars or ribbons. The particle size and particle size distribution have been quite varied, and no extensive studies exist on their influence on the composite properties, neither on damping nor on the maximum shape change. Several polymer matrices, such as epoxies, polyesters, polyurethanes, and silicones, have been used as a polymer matrix. In most studies, the Ni-Mn-Ga particles have been aligned by an external magnetic field during the curing, which tends to align the Ni-Mn-Ga particles into chains, and optimize the composite for a shape change. However, in particular at high loading levels, the aligned chains can decrease the mechanical properties of the composites by cracking. [28-34] A model to estimate the maximum shape change in polymeric composites has been developed for Ni-Mn-Ga. The model gives an upper limit value of strain as 21% of the maximum shape change for randomly orientated particles, when compared to bulk single crystal Ni-Mn-Ga. For field-aligned particles, the upper limit value is 50%. Although several studies have been carried out with Ni-Mn-Ga powder/polymer composites, and improved damping capability has been reported, no study has shown any significant shape change with these composites. With laminate structures, constructed on single crystal plates or rods bonded with polymers, such as epoxies or polyurethanes, a low level shape change (about 20% of the theoretical) has been achieved.[8, 35-36] Some novel ideas have been suggested to overcome these limitations in composite design, the most promising results have been obtained with porous metallic foams. With metallic foams, shape changes of up to several percent have been found, which is actually higher than the theoretical values for polymer based composites.[37]

1.3 Carbon nanotubes (CNTs) and their polymeric composites

1.3.1 Carbon nanotubes

Graphene, fullerenes and carbon nanotubes (CNTs) are all allotropes of carbon. Fullerenes (buckyballs) are molecules, composed of carbon which is arranged in hexagonal and pentagonal rings, which can form hollow spheres, resembling a soccer ball. Graphene on the other hand is a planar sheet of carbon atoms arranged in hexagonal rings. CNTs are a combination

of both graphene and fullerene; the tube is a rolled-up sheet of graphene with a half fullerene cap. The cap is usually removed during the initial cleaning of CNTs. There are two main structures of CNTs: single-walled CNTs (SWCNTs) and multi-walled CNTs (MWCNTs). SWCNTs only have one wall (graphene sheet), so they have a small diameter (from 0.4 nm to 4 nm, often ~ 1.2 nm). Depending on their chirality, SWCNTs can be either metallic (one third) or semiconducting (two thirds). MWCNTs, on the other hand, are composed of several walls, the quantity of the walls ranging from 2 (so called double-walled CNT, DWCNT) to less than 100. The diameter of MWCNTs is varied, but usually, their diameter is in the range of 10-50 nm. MWCNTs are practically always metallic, as 1/3 of the SWCNTs are metallic. It is possible to grow monochiral MWCNTs, where all the walls have the same chirality, but commercial MWCNTs are not monochiral. Ideally, crystalline SWCNTs and MWCNTs have walls without any defects, such as missing or added atoms. In practice this is not the case, MWCNTs in particular have defects in their structure. CNTs can be manufactured by three industrial-level methods. Arc discharge and laser ablation methods are high-temperature methods, where the carbon source is heated rapidly, either by an electrical current (arc discharge) or by laser (laser ablation). Both methods can produce substrate-free CNTs with good, or even excellent, crystallity control. The major drawback for both methods is that the CNTs need to be separated from other carbon products and other residues. The main technique for industrial level CNT production is chemical vapour deposition (CVD). CVD requires a significantly lower temperature (usually 700-900 °C, but lower temperatures have been tried with varying success), and it allows growing the CNT directly in-place. CNT synthesis by CVD is based on the catalytic decomposition of carbon-containing gases on Fe, Co, or Ni in the form of thin films or as deposited nanoparticles. CVD allows the synthesis of long CNTs, but as the processing temperature is lower than for an arc discharge or laser ablation, the CNTs usually have more defects. The post-separation of CNTs from other carbon products, on the other hand, is significantly simpler or may even be completely avoided. With CVD, the CNTs can be mass-produced at a reasonable price for applications.[2, 38-39]

1.3.2 Carbon nanotubes and their dispersion in polymers

Pristine nanotubes always exist as bundles. As with all chemical components, van der Waals forces are responsible for close range attraction between individual CNTs. Usually, the attraction by van der Waals forces is

weak. However, CNTs have a very high aspect ratio (up to thousands) and so they have extraordinary high van der Waals forces hindering the break up of CNTs bundles. The CNTs will also easily re-aggregate, if the dispersing force is removed. As the dispersion of fillers into a polymer matrix is a key element in composite design, the dispersion of CNTs has been studied intensively during the last two decades. There are five basic methods to disperse CNTs into a polymer matrix: (1) dispersion into a liquid monomer, followed by a reaction; (2) both polymer and CNTs are dissolved into the same solvent separately, followed by dispersion and precipitation; (3) monomer and nanotubes dispersed into a liquid, which is then evaporated; (4) CNTs mixed with a polymer melt; (5) CNTs mixed with a solid polymer. Many of these dispersion methods require the use of organic solvents, which must be removed afterwards, leading to additional processing steps and higher costs. Two widely used methods to produce CNT-based composites are the direct melt mixing of a matrix polymer and CNTs by an extruder and *in situ* polymerization of, for example, styrene or methyl methacrylate in the presence of CNTs. The dispersion of CNTs with melt mixing is based on shear forces during the mixing procedure; the dispersion quality of direct melt mixing is often limited, but the method is quick and easy to implement. *In situ* polymerization with CNTs generally provides better dispersion, but requires additional processing steps. *In situ* polymerization, in the presence of CNTs, requires the use of a surfactant agent, which is able to prevent the re-agglomeration of CNTs. The initial break up of the bundles is often carried out with ultrasonication, as the mechanical mixing cannot provide enough energy to break the bundles in a solvent. Traditional surfactants for emulsion polymerization, such as sodium dodecyl sulfate (SDS) and sodium dodecyl benzene sulfate (DBSA), can be used in the polymerization of CNT-based polymer composites. The surfactant molecules are attached onto the CNT surface and will prevent the CNTs from contacting each other.[3,41-44] Besides basic surfactants, other molecules, such as amphiphilic block copolymers, have been used to disperse CNTs. Their working principle is to wrap around the CNTs and thus prevent their re-agglomeration by steric influence.[45-47] A widely used method to enhance the dispersion of CNTs into a polymer or solvent is to use functionalized CNTs. The functionalizing agent is attached to the surface of the CNT, the CNT re-agglomeration is restricted, and the solubility of CNTs is enhanced. Also, with a property designed functionalization agent, the matrix polymer and CNTs can be covalently bonded, meaning better mechanical properties for the composite. The negative effect, especially for a sidewall functionalization, is the interruptions in the π-π network, which leads to a lowered electrical

conductivity of CNTs. Besides mechanical properties and electrical conductivity, the thermal conductivity is an essential property of CNT-based polymer composites, which can be enhanced with the addition of CNTs.[48-50]

1.4 The scope of the thesis

Composites, and especially nanocomposites, have been studied extensively by the Polymer Research Group at Aalto University. The aim of this thesis was to produce polymeric composites with Ni-Mn-Ga and carbon nanotubes, and to study the properties of the produced composites. Ni-Mn-Ga alloy is expensive to produce, and limited in size and form due to production restrictions. The goal about Ni-Mn-Ga/polymer composites was that by combining a polymer matrix with Ni-Mn-Ga in powder form, the price of the product with still sufficient level of properties like damping could be lowered, and the size and form limitations could be eliminated. With CNT/polymer composites the goal was to obtain a good dispersion of CNTs in polymer matrix which has been proven to be a difficult task, and which is one of the main obstacles restraining large-scale industrial use of CNTs in polymer composites. Ni-Mn-Ga had a large particle size (microscale), while carbon nanotubes were at a nanoscale, meaning that the preparation of the composites and how to achieve effective filler dispersion varied greatly.

This thesis summarizes the research reported in six publications, I-VI, supported by some unpublished data. The first part of the study (publications I-II) focused on studies on temperature and stress dependency on damping of bulk Ni-Mn-Ga (10M and NM). Both properties are critical factors when designing polymeric composites with damping or actuating capabilities.

Ni-Mn-Ga/polymer composites were studied in III, some research data is unpublished. The studies of material properties, such as polymer matrix strength, the adhesion between Ni-Mn-Ga and a polymer matrix, were combined with studies of Ni-Mn-Ga powder orientation in composite in magnetic field. The damping properties of the composites were studied using dynamic mechanical analysis (DMA). Also, a magnetic circuit was designed and built for the DMA system, in order to measure the active damping of Ni-Mn-Ga/polymer composites under a magnetic field.

In the second part of the thesis, IV-V, carbon nanotubes were *in situ* polymerized with methyl methacrylate. Two types of dispersing agents, traditional anionic (IV) and amphiphilic copolymers (V) were used, and their carbon nanotube dispersing capabilities and influence on polymerization were studied. The carbon nanotubes were found to take part in polymerization process and thus, affect the molecular weight of the PMMA. The mechanical properties, electrical and thermal conductivities of the composites were studied. The dispersion of CNTs into a polymer was studied by electron microscopy.

In VI, the CNT/PMMA composites (from IV) were used as a masterbatch and added into commercial PMMA by extrusion. Composites with CNTs dispersed directly into commercial PMMA by extrusion were also manufactured, and compared to masterbatch-based composites. The effect of a matrix viscosity on the percolation threshold was also studied by adding glycerol into masterbatch-based composites, thus, lowering the viscosity.

2. EXPERIMENTAL

2.1 Materials

2.1.1 Materials for bulk Ni-Mn-Ga studies

Several Ni-Mn-Ga alloys with different crystal structures were used in temperature and stress dependence studies. All of the test materials were produced by directional solidification at Outokumpu Research, Inc. and Adaptamat Ltd. The produced ingots were annealed in the vacuum quartz ampoules, first for 48 hours at 1253 K, and then for 72 hours at 1073 K for structural homogenization. Specimens were then cut from the ingot by spark machining, mechanically polished and finally electropolished in 25% HNO_3 to reduce surface stresses built up during the cutting and to enable the twin boundary motion. A summary (chemical compositions, phase transformation (M_s, M_f, A_s, A_f) and Curie (T_c) temperatures, and primary martensite structure) of used bulk Ni-Mn-Ga specimens is given in Table 1.

Table 1. A summary of the bulk Ni-Mn-Ga alloys and their chemical compositions, phase transformation and Curie temperatures used in this study. [I,II]

Specimen	Ni (at. %)	Mn (at. %)	Ga (at. %)	M_s (K)	M_f (K)	A_s (K)	A_f (K)	T_c (K)	Crystal structure	Publication
A1	48.9	30.0	21.0	311	297	313	320	375	mixed	I
A2	49.7	29.1	21.2	307	300	316	320	372	10M	I
A3	55.1	22.1	22.9	374	367	376	386	377	NM	I
A4	52.3	27.4	20.3	407	400	410	418	380	NM	I,II

2.1.2 Materials for Ni-Mn-Ga/polymer composites

Several types of composites (publication III and some unpublished results) were produced with different matrix polymers and different forms of Ni-Mn-Ga (powders, ribbons and bulk). A summary of the used polymer matrix, inserted Ni-Mn-Ga material, and composite type is given in Table 2. All of the matrix polymers were supplied by Henkel KGaA.

Table 2. A summary of the Ni-Mn-Ga/polymer composites studied. [III, unpublished *]

Inserted material	Matrix polymer	Composite type	Transformation temperatures of inserted material (K) / crystal structure
$Ni_{49}Mn_{27}Ga_{24}$ powder 15 vol-%	Epoxy Hysol 9455	Powder in polymer matrix	M_S 309, M_f 299, A_s 303, A_f 316, T_C 371 / 10M martensite
	Epoxy Hysol 9492		
	Silicone Loctite 5140		
Reference samples with Ni, Fe, or Cu powder 15 vol-%	Epoxy Hysol 9455	Powder in polymer matrix	
	Epoxy Hysol 9492		
	Silicone Loctite 5140		
	Epoxy Hysol 9455	Polymer reference samples	
	Epoxy Hysol 9492		
	Silicone Loctite 5140		
$Ni_{49}Mn_{30}Ga_{21}$ powder 50 vol-% *	Epoxy Hysol 9484	Powder in polymer matrix	M_S 326, M_f 320, A_s 330, A_f 337 / 10M martensite
$Ni_{49.3}Mn_{29.9}Ga_{20.8}$ R1 rapidly cooled ribbon	Epoxy Hysol 9455	Sandwich geometry	M_S 306, M_f 291, A_s 299, A_f 314, T_C 372 / 10M martensite
$Ni_{51.6}Mn_{30.0}Ga_{18.4}$ R2 rapidly cooled ribbon	Epoxy Hysol 9455	Sandwich geometry	M_S 357, M_f 339, A_s 344, A_f 360, T_C 366 / 14M martensite
$Ni_{52.3}Mn_{27.4}Ga_{20.3}$ bulk	Epoxy Hysol 9455	Bulk/epoxy composite	M_s 406, M_f 394, A_s 409, A_f 420, T_C 373 / Non modulated

Ni-Mn-Ga powders, expect $Ni_{49}Mn_{30}Ga_{21}$ powder used with Epoxy Hysol 9484, were produced from melt-spun Ni-Mn-Ga ribbons with dry ball-milling at room temperature using steel balls. $Ni_{49}Mn_{30}Ga_{21}$ powder used with Epoxy Hysol 9484 was produced from single crystal bar via ball-milling. As the milling produced a significant amount of thermal energy, the actual milling temperature was probably significantly higher than the room temperature. At least 10M martensites were in an austenite region during the ball-milling. This produced a more homogenous particle size, and the milling time could be shorter in an austenite region. In a martensite region, the twin boundary motion consumes part of the milling energy, especially with 10M martensites. The twin mobility for $Ni_{49}Mn_{30}Ga_{21}$ powder used with Epoxy Hysol 9484 was improved by mechanical

compression. Compression promotes the preferred martensite variant to occur along the compressive stress. For other Ni-Mn-Ga powders and ribbons, no compression treatment was carried out. Particles over 150 μm, except in the case of the $Ni_{49}Mn_{30}Ga_{21}$ powder used with Epoxy Hysol 9484, were sieved from the prepared powder; their morphology was not studied. In the case of $Ni_{49}Mn_{30}Ga_{21}$ powder with Epoxy Hysol 9484 range of 150-300 μm was used. After the ball-milling, the materials were annealed at 1073 K, as the powder contained a large amount of dislocations and stresses. In addition to the Ni-Mn-Ga powder, Ni (Osprey Metals Ltd.), Cu (Merck), and Fe (BDH Chemicals) powders were used as reference materials. Particles with a diameter of over 150 μm were removed from the reference materials. The Ni particles were round, whereas the other powder particles were random in shape.

Weighted amounts of the polymer component (40, 85 or 100 vol-%) and Ni-Mn-Ga powder were mixed by hand and poured into a polytetrafluoroethylene (PTFE) mould at room temperature. Silicone-based composites were placed in a temperature-controlled room (air humidity ~ 50 % and temperature ~ 296 K) to speed up the sample curing. In the case of $Ni_{49}Mn_{30}Ga_{21}$ powder used with Epoxy Hysol 9484, an external magnetic field was used during the curing to orientate the Ni-Mn-Ga particles; with other composites, no external magnetic field was used.

Two rapidly cooled ribbons with transformation regions close to room temperature (R1) and in a higher range (R2) were used in sandwich-type laminates. The ribbons were manufactured by melt-spinning from a polycrystal ingot and heat treated for 24 h at 1073 K in vacuum quartz ampoules. Composites with a sandwich geometry consisted of about 20 layers of thin Ni-Mn-Ga ribbons embedded in very thin layers of epoxy. Such a laminate structure was necessary because the individual ribbons were brittle. In the case of bulk composites, thin bulk Ni-Mn-Ga plates were cut from a single crystal piece. Since the size of the raw material limited the sample preparation, the cutting was not performed along a specific crystallographic plane. After curing, the samples were cut with a diamond saw. The samples consisted of three plates, interspaced by two epoxy layers.

2.1.3 Materials for CNT/polymer composites

Two MWCNT types were used: Nanocyl NC7000 and Bayer C 150 HP (Bayer Baytubes). Nanocyl NC7000 (Nanocyl S.A., Belgium) has a carbon

purity ~90 %, an average diameter ~ 9.5 nm, and an average length ~ 1.5 microns. Bayer C 150 HP (Bayer, Germany) has a carbon purity >99 %, an average diameter 13-16 nm, and an average length ~ 1 micron. The double-walled carbon nanotubes (DWCNT) NC2100 (Nanocyl S.A., Belgium) has a carbon purity >90 %, an average diameter ~ 3.5 nm, and an average length 1-10 microns. The given purities, and average diameters and lengths are based on data provided by the manufacturers. All three of the CNT types are manufactured via a chemical vapor deposition (CVD) process. In most polymerizations, the CNTs were used as received. For some polymerizations, the CNTs were acid functionalized.[51]

The monomer, methyl methacrylate was supplied by Fluka (Sigma-Aldrich). The monomer was treated with aluminum oxide (supplied by Fluka) to remove the inhibitor. The initiators, potassium peroxodisulfate (KPS) and azobisisobutyronitrile (AIBN) were supplied by Fluka (Sigma-Aldrich). The surfactants, sodium dodecyl benzene sulfate (DBSA, Fluka) and sodium dodecyl sulphate (SDS, Sigma-Aldrich), and the buffer, sodium hydrogen carbonate ($NaHCO_3$, Merck), were used as received. Plasticizer, glycerol (Merck) was used as received.

For extrusion studies (publication VI), commercial poly(methyl methacrylate) (IG840, LG Chemicals) was used. The polymer was milled before extrusion.

The cationic copolymers used as surfactants in publication V, poly(stearyl methacrylate-*stat*-dimethylaminoethyl methacrylate)s were synthesized with radical polymerization. The amino groups were quaternized into the cationic form in order to increase water solubility. The poly[(stearyl methacrylate)-*stat*-([2-(methacryloyloxy)ethyl] trimethyl ammonium iodide)] was water-soluble when the amount of stearyl methacrylate (SMA) was less than 17 mol%.[52]

2.2 The polymerization of CNT/polymer composites

Carbon nanotubes, surfactant, buffer $NaHCO_3$, and distilled water were introduced into a flask, cooled in an ice bath and the mixture was deoxygenated by bubbling with argon. Ultrasonic treatment was carried out with the probe of an ultrasonic horn immersed directly into the mixed system. After the ultrasound treatment, the flask was transferred into an oil bath and fitted with a stirrer, using a stirring rate of 300 rpm. In the case of

KPS as an initiator (emulsion polymerization), the KPS was dissolved in water and the solution was fed into the reactor before the monomer. The monomer was added drop by drop with a membrane pump at 0.03 mL/min. In the case of AIBN as an initiator (combined emulsion/suspension polymerization), the AIBN was dissolved in the monomer and the solution was fed into the reactor with the membrane pump at 0.03 mL/min. The polymerizations were carried out at a temperature of 65 °C (KPS as an initiator), and at a temperature of 75 °C (AIBN as an initiator). The polymerization times were 20-21 h. After polymerization, the emulsion was dried in an oven at 50 °C for at least 48 hours.

2.3 Melt mixing procedure for CNT/polymer composites

Composites were prepared with a corotating twin-screw midiextruder (DSM, capacity 16 cm^3, screw length 150 mm) under nitrogen atmosphere. Composites were mixed at 120 rpm and 10 min at 210 °C. The CNT content in the composites was 1 – 4 wt.% and the CNTs were incorporated directly or by using a masterbatch-approach.

2.4 Characterizations

2.4.1 The characterization of bulk Ni-Mn-Ga

The crystal structure and orientation of bulk Ni-Mn-Ga material were determined by X-ray diffraction at room temperature (Philips X´Pert) using Co K_α radiation.

The chemical composition of used Ni-Mn-Ga alloys was measured by scanning electron microscopy (SEM) and energy-dispersive X-Ray microanalysis (EDS).

The Ni-Mn-Ga phase transformation temperatures were measured with differential scanning calorimetry (either Linkam DSC 600 or Shimadzu SC-50) with a heating rate of 4 K/min. The Curie temperature was measured with low-field AC magnetic susceptibility measurement.

The damping properties of the bulk alloys were studied by using the Perkin–Elmer Dynamic Mechanical Analyser DMA-7. The configuration used was three-point bending (3pb) with the specimen in the horizontal

position. The dimensions of the rectangular specimens varied significantly and, thus, a different amount of force had to be applied to achieve high enough amplitude. It is possible that a different force level had a slight effect on the measured modulus. The initial applied amplitude was 3-5 μm and the amplitude was limited to 25 μm. The DMA measurements were performed at a fixed 1 Hz frequency at a zero magnetic field and the applied temperature range depended on the transformation temperatures of the sample. The cooling and heating were carried out at rate of 4 K/min. Sample A4 was also tested (publication II) with another DMA system (DMA Q800 from TA Instruments). A single cantilever mode with a frequency 95 Hz at a zero magnetic field was used for stress testing. A higher frequency was used, as the target range for Ni-Mn-Ga based applications, for example actuators, can be up to tens or even hundreds of Hz.

2.4.2 The characterization of Ni-Mn-Ga/polymer composites

The adhesion between the polymers and the bulk $Ni_{52.4}Mn_{27.3}Ga_{20.3}$ alloy was analyzed at room temperature with a specific laboratory test configuration (publication III). The Ni-Mn-Ga surfaces were finished with 800 grit sandpaper before joining with the specimen holders; the studied polymer was then applied between two holders. Five pairs of specimens were used in the tensile shear stress test to compare the adhesion of the polymers.

The damping properties of the Ni-Mn-Ga/polymer composites were studied by DMA. The temperature scans for composites were mainly run with Perkin–Elmer Dynamic Mechanical Analyzer DMA-7. The parallel plate (PP) configuration was used for the softer polymer composites with Hysol 9455 epoxy and for the Loctite 5140 silicone, whereas, for the hard Hysol 9492 based materials, a three-point bending (3pb) configuration was used. For ribbon composite samples (R1 and R2), three-point bending geometry was used. All these DMA measurements were performed at a fixed 1 Hz frequency in a zero external magnetic field. The heating rate was 4 K/min. The bulk thin-plate Ni-Mn-Ga/Hysol 9455 composite samples were measured with other DMA equipment, a Rheometric Scientific DMTA V, in a single cantilever mode at room temperature. The frequency used for these samples was 20 Hz.

10M martensite based epoxy composites were tested under a magnetic field by the TA DMA Q800 system. The magnetic circuit was assembled to the

DMA unit, so that the single cantilever beam geometry could be used for the sample under a magnetic field. The relatively low field strength, 0.31 T, could not be increased due to the DMA design limitations. The working principle was that the 10M martensite would be magnetized to reorientate with the c-axis transversal to the strain at the sample surfaces. The reorientation of the twins was triggered by the magneto-stress along the field, and the created magneto-stress should be overcome by the bending stress by DMA.

Glass transition temperatures (T_g) were measured by DMA for Ni-Mn-Ga/polymer composites with temperature scans (publication III), and were approximately 310 K for Epoxy Hysol 9455, 349 K for Epoxy Hysol 9492, and below 253 K for Silicone Loctite 5140. For Hysol 9484, all DMA measurements were done at room temperature. The glass transition temperature for Hysol 9484 was 329 K (manufacturer data, ASTM D 1640).

2.4.3 The characterization of CNT/polymer composites

The morphology of the composites and dispersion of MWCNTs were studied with transmission electron microscopy (TEM). The samples were sectioned with an ultramicrotome and diamond knife at room temperature. Approximately 70 nm thick sections were collected on copper grids. Either a Tecnai 12 Bio Twin at room temperature or a Jeol JEM-3200FSC cryo-transmission electron microscope at -188 °C was used for TEM studies. Both were operating in a bright field mode, using an acceleration voltage of 120 kV (Tecnai 12 Bio Twin) or 300 kV (Jeol JEM-3200FSC). Also, scanning electron microscopy (FE-SEM, Jeol JSM-6335F) was used to study the morphology of composite samples. The hot pressed composite specimens were fast frozen in liquid nitrogen and fractured. The fractured surface samples were coated with chromium, in order to stabilize the samples under the electron beam and to enhance the image contrast. The electron micrographs were taken using an acceleration voltage of 5.0 kV.

Molecular weights (M_w) and molecular weight distributions (PD) were determined with respect to polystyrene standards by size exclusion chromatography (SEC, The Waters Associates system). The dried samples were dissolved in chloroform, which was also used as an eluent in SEC. Samples were filtered twice through a 450 nm (pore size) filter to remove the insoluble components. Room temperature was used for all the SEC analyses.

The mechanical properties of the composites (publications IV and V) were analyzed by DMA (TA Instruments Q800) at 25 °C, using a single cantilever 20 mm (effective length 10 mm) probe from hot pressed specimens. The glass transition temperature of composite specimens was measured with DMA, using a heating rate of 3 °C/min from 0 °C to 180 °C (publications IV and V). Temperature runs were done in the amplitude mode (50 μm). A frequency of 1 Hz was used for all the tests.

The mechanical properties of the composites for extrusion studies (publication VI) were characterized from hot pressed specimens. Tensile tests were performed with an Instron 4202 testing machine, using a test speed of 5 mm/min and with the specimen type 1BA, according to the standard ISO 527:1993(E).

For extrusion studies (publication VI), differential scanning calorimetry (Mettler Toledo DSC 821), using a heating rate of 10 °C/min from 25 °C to 220 °C, was used to measure the glass transition temperatures, T_g.

The melt rheology properties of the PMMA composites (publication VI) were determined indirectly from the final composites, by using a rotation rheometer (Anton Paar Physica MCR 301) with a parallel plate geometry, gap 0.4 mm, at 210 °C, using dynamic oscillation frequency sweeps of 0.1 – 100 rad/s under a nitrogen atmosphere.

Electrical conductivity was measured directly from the surface of hot-pressed specimens by the four-probe method (Keithley 2400 Sourcemeter). The distance between the probes was about 1 mm. The specimen surfaces were finished with grit 600 paper to remove any possible polymer layer. The thermal conductivity was measured from hot pressed (diameter 12 mm, thickness 2 mm) specimens using a Hot Disk Thermal Constants Analyzer combined with the Keithley 2400 Sourcemeter. The thermal conductivity specimens were stabilized for 30 minutes; the measurement was done at 0.05 W for 30 seconds.

3. RESULTS AND DISCUSSION

3.1 Ni-Mn-Ga bulk and vibration damping [I, II]

Shape changing metal alloys, such as Ni-Mn-Ga and Cu-Al-Ni, usually have high damping capabilities, which can be controlled via an external factor, like temperature or a magnetic field. Beside material properties, the damping capability depends on the type of the external vibration (frequency, waveform, amplitude etc.). For Ni-Mn-Ga, a higher frequency tends to give a higher damping capability, if the alloy or composite structure can sustain the strain. Ni-Mn-Ga alloys have their transformation temperature (martensite to austenite), which can be utilized in passive damping. In practice, a conventional SME is not very usable, since the SME depends on a temperature change over a transformation temperature, which is a slow process. An external magnetic field, however, has been reported to have a slight influence on transformation temperature; this might enable the utilization of SME with a faster response. A more usable way to utilize Ni-Mn-Ga alloys in vibration damping is to use an external magnetic field with a suitable Ni-Mn-Ga alloy structure in a martensite phase. [53-60] The upper temperature limit of MSME is the transformation to austenite or the Curie temperature, the lower limit of MSME has not been thoroughly studied, some reports have given the values ~ 165 K for 10M Ni-Mn-Ga alloys.[61-62]

Figs. 2 and 3 show the storage modulus E' (corresponds to the real part of the complex modulus and represents the elasticity of the material), loss modulus E" (corresponds to the imaginary part of the complex modulus and represents the ability of the material to "lose" energy), and tan δ as a function of the temperature during heating (denoted by h) and cooling (denoted by c). Sample A2 had 10M martensite structure and sample A3 was non-modulated (NM) martensite. The damping (tan δ) for both samples was significantly higher in the martensite phase than in the austenite phase, as expected, as in the austenite phase, there was no twinning and therefore no significant damping mechanism.

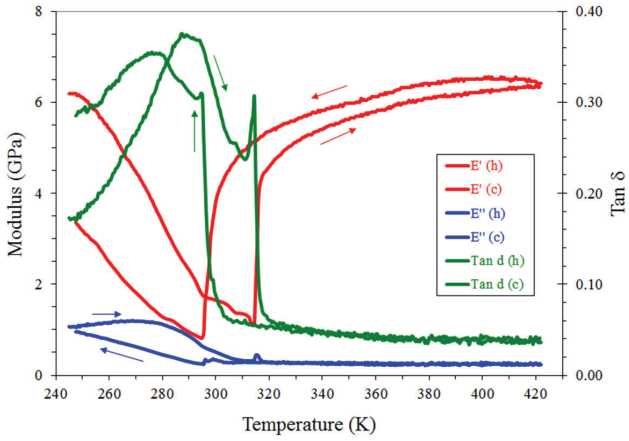

Fig. 2. DMA measurements (storage modulus E', loss modulus E'' and damping Tanδ) of the sample A2 (10M martensite) as a function of temperature (→ representing heating direction of the thermal cycle, ← representing the cooling direction of the thermal cycle). [I]

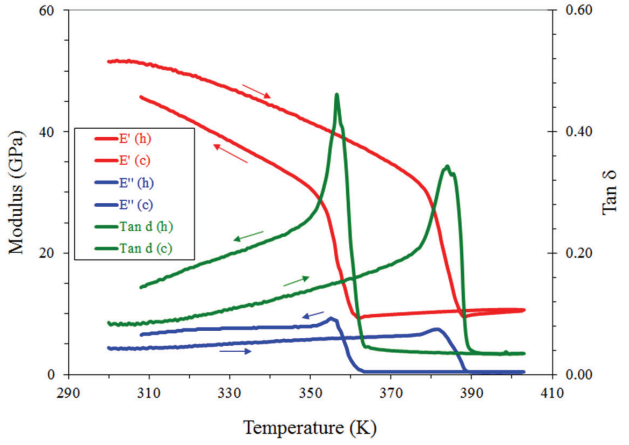

Fig. 3. DMA measurements (storage modulus E', loss modulus E'' and damping Tanδ) of the sample A3 (non-modulated martensite) as a function of temperature (→ representing heating direction of the thermal cycle, ← representing the cooling direction of the thermal cycle). [I]

At the martensite to austenite transformation, the storage modulus E' of the samples showed a decrease accompanied by a sharp peak of tan δ. Loss modulus E'' stayed nearly constant in the martensitic phase. At the martensite to austenite transformation, there was a small but noticeable

peak of loss modulus E", which suggested an increase of the damping due to movable phase boundaries or stress induced martensite formation. The peak of tan δ was much larger due to the decrease of the storage modulus E'. The values of storage modulus differed sharply, ranging from a few GPa to above 100 GPa. This reflected the different martensite structures (10M or NM). The high damping in sample A2 was due to a high mobility of the twin boundaries in a 10M martensite. When cooling from austenite, after the initial peak in tan δ denoting the transformation, sample A2 (10M) showed in particular another peak after transformation and then tan δ decreased again. The decrease of tan δ with a decreasing temperature reflected the decreasing mobility of twin boundaries with decreasing temperature. Sample A1 and, to some extent, sample A4 (publication I) showed a rather broad temperature evolution of measured values, probably due to sample inhomogeneity. A very sharp transformation in A2 and A3 samples indicated higher homogeneity and a single crystal structure. After the DMA thermal cycle, tan δ remained at a higher level compared to the initial value, especially for NM samples. This might be a result of a re-orientation of the martensite structure during the DMA cycling, similar to "normal" Ni-Mn-Ga training. For all the samples, 10M, NM and mixed, the increase in temperature enabled an increasing motion of twin boundaries in the martensite region, which in turn led to a higher capability of vibration damping, as the material was able to dissipate additional vibration energy.

Ni-Mn-Ga alloys have a certain level of stress (twinning stress), which must be exceeded before the shape change by an external magnetic field or force can be realized. This stress dependence of the modulus and damping was measured by DMA for an NM martensite sample. In the martensite region, the modulus values decreased along with increasing stress. In the austenite region, the modulus values were stable. This indicated a twin boundary motion, where the increasing stress led to modulus softening and easier movement for the twins, which is the main contributor for damping for NM martensites. A similar trend was found for damping (tan δ). The damping capability for NM martensite (publication II) is shown in Fig. 4. The damping (points without a connecting line) in the martensite region was low at low stress, and only slowly increased along with increasing stress, until a certain stress level was obtained and the damping capability of the Ni-Mn-Ga alloy started to increase more rapidly. For an NM martensite, the required stress is up to tens of MPa (about 20 MPa for the NM martensite measured in publication II), for 10M and 14M martensites, the required twinning stress was not measured, but is significantly lower, usually 1-3 MPa. Both the temperature (publication I) and stress (publication II) has a

significant influence on the modulus and damping capability of Ni-Mn-Ga, and they are important factors when developing applications or composites based on Ni-Mn-Ga alloys.

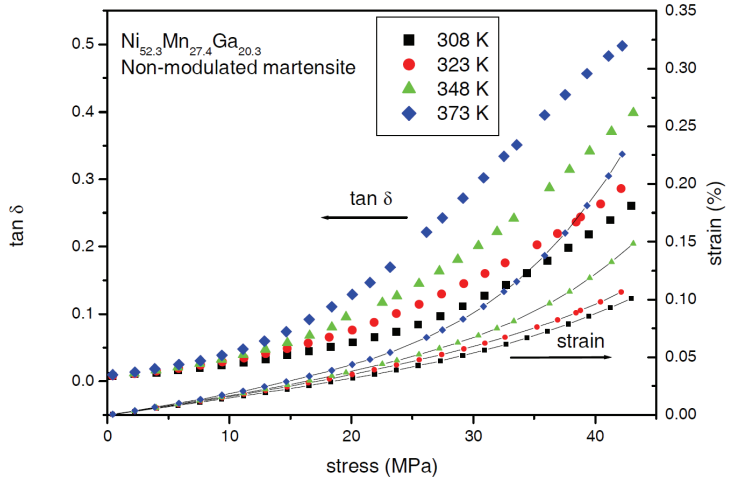

Fig. 4. Tan δ (points) and maximum measured strain (connected by a line) for NM martensite as a function of stress in a martensite phase. [II]

3.2 Ni-Mn-Ga/polymer composites [III]

Based on information obtained from Ni-Mn-Ga bulk damping studies, several types of Ni-Mn-Ga/polymer composites were manufactured and studied. Besides damping, good adhesion between a polymer matrix and Ni-Mn-Ga component is essential for the composites, especially at temperatures which are close to or even above the glass transition temperature of the polymer (T_g). Few research groups have used silane coupling agents and plasma treatments, combined with different polishing treatments, to enhance the adhesion between Ni-Mn-Ga and Ni-Ti powders and polymers. When applied alone, the silane coupling agents did not have a significant influence on the adhesion; plasma treatments of Ni-Ti improved the adhesion.[63-64]

In this study, a silane coupling agent (Oxsilan mm 0705) was tested, but no significant improvement on the adhesion, or mechanical properties, were found (unpublished results). As the testing with the silane coupling agent did not improve the composite properties, the silane was not used for the manufactured composites. After the initial ball-milling, the Ni-Mn-Ga powder was heat treated and stored under a normal atmosphere and an oxide layer formed onto the surface of the powder particles. The thickness of the oxide layer on the various sized and random shaped particles was not

measured, there might be significant variation. The oxide layer on the Ni-Mn-Ga powder surface probably had an influence on the powder/polymer adhesion. Adhesion tests were carried out at room temperature (publication III). Epoxies had good adhesion between the matrix and particles. The silicones had only a low level of adhesion. Some polyurethanes were also tested for adhesion, but the adhesion between the polyurethanes and Ni-Mn-Ga particles was very poor.

Based on results from the adhesion tests, epoxies were selected as the matrix material. The selected epoxies were all two-component and self-hardening. Traditionally, epoxies are baked at an elevated temperature to ensure that the curing is complete. With Ni-Mn-Ga, however, there were restrictions with the baking approach. The phase transformation temperature of the Ni-Mn-Ga set a limit for the maximum heat treatment temperature. In order to retain the magnetic orientation of the powder, the heat treatment needed to be conducted below the A_s temperature of Ni-Mn-Ga, which is rather low for the 10M type martensite structures. For NM martensites, the limiting A_s temperature is higher. Due to this limitation, the total cure of epoxies could not be carried out, and some post-curing took place after the composite preparation.

Epoxy Hysol 9455 was mixed with $Ni_{49}Mn_{27}Ga_{24}$ powder (15 vol-%, no magnetic field was used during curing). The damping results are shown in Fig. 5. All of the composite samples (Ni-Mn-Ga and reference materials) had a higher damping capacity than the pure epoxy. The damping of the Ni-Mn-Ga powder/polymer composite improved at 310 K, i.e., just above the T_g of the polymer, but at about 318 K, the damping dropped again sharply. This temperature region corresponded well with the martensite to austenite transition of the Ni-Mn-Ga alloy used. A comparable composite was prepared with epoxy Hysol 9492, which was a significantly tougher material after curing. No detectable change was seen in the damping in the 303–323 K range. With epoxy Hysol 9492, the Ni-Mn-Ga particles were too constrained in the epoxy and could not deform, and the composite did not show any additional damping in the martensite to austenite transition area. A similar composite was prepared with silicone, which showed low adhesion when tested. However, no clear change occurred in the 303–323 K range. Only a very weak change could be observed in the Ni-Mn-Ga powder/polymer composite at about 311–317 K. Apparently, the silicone material was too soft, compared to the Ni-Mn-Ga powder. The polymer matrix yielded around the Ni-Mn-Ga particles, and the damping energy was transferred inefficiently. Epoxy Hysol 9455 was used with ribbon sandwich

composites. For both of the Ni-Mn-Ga alloys used, R1 and R2, tan δ showed some extra damping at the phase transformation region.

Several requirements for a polymer matrix were realized from the DMA results of the composites. If a high damping capacity is required, the matrix polymer of the composite must be closely equivalent to the mechanical properties of the Ni-Mn-Ga component. Similar findings have been proposed for silicones and polyurethanes,[65] the problems have also been studied by using an mathematical approach.[66] With 10M type martensites, this means a relatively low yield stress; the typical stress which is needed to move the twin boundaries is usually 1 - 3 MPa. With an NM type martensite filler, the matrix should have a yield stress of about 20 MPa or higher. With mixed or inhomogeneous Ni-Mn-Ga, the effective design of a high damping composite will be very difficult, as the properties, including those which are mechanical, of the Ni-Mn-Ga alloy can vary greatly.

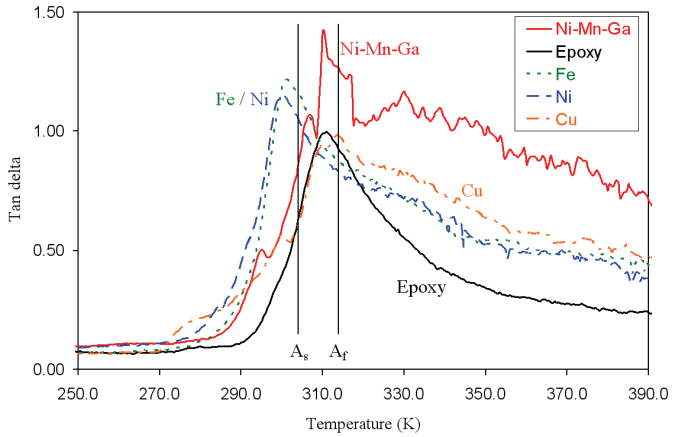

Fig. 5. Damping (tan δ) for epoxy Hysol 9455/$Ni_{49}Mn_{27}Ga_{24}$ powder (15 vol-%, no magnetic field was used during curing) composite as a function of temperature. [III]

In order to increase the damping capability of Ni-Mn-Ga based polymer composites, the powder loading was increased (up to 60 vol-%) and the Ni-Mn-Ga powder was oriented in the magnetic field during the curing process. By curing the composite under a magnetic field, the Ni-Mn-Ga powder could be oriented, but the matrix polymer must have a suitable viscosity. An improved alignment of SMA particles has been reported for both Ni-Mn-Ga powder and Terfonol-D ($Tb_xDy_{1-x}Fe_2$, commercial magnetostrictive material). Oriented SMA powder has a larger shape memory change than non-oriented powder.[67-71] Furthermore, to enable damping studies under an active magnetic field, a magnetic circuit,

generating a 0.31 T magnetic field, was enabled for DMA measurements. The magnetic field strength of 0.31 T was low, as the reported values of the saturation magnetic field for 10M martensites are in the range of 1-7 T.[8] The magnetic field strength of 0.31 T was probably only able to activate the most easily movable twins, twins with even a slightly locked position were most likely not activated. The DMA measurement mode which was used was a single cantilever, which was a more suitable choice for active damping testing under a magnetic field with the composites. The basic actuator design with Ni-Mn-Ga first has the transforming phase and then the twins are driven back to the original state. The single cantilever mode simulates an actuating cycle better than a 3-point bending mode.

To estimate the difference in active damping between a pure polymer (epoxy Hysol 9484) and a Ni-Mn-Ga/polymer composite, stress-strain tests were run at room temperature with DMA. Both the pure polymer and the composite samples were baked in an oven at 323 K for 24 h, higher temperatures could not be used as the variant orientation would have been lost. Fig. 6 shows damping (Tan δ) versus stress under a 0.31 T magnetic field, emulating active damping. The pure polymer did not show a significant increase in damping under increasing stress levels. The composite (60 vol-% load), on the other hand, did show an increase in damping at higher stress levels (> 1 MPa). For the composite, the storage modulus values decreased with an increasing stress level, corresponding to modulus softening and easier movement for the twins, similar to bulk NM martensites (publication II). The increased damping at a higher stress level correlated well with bulk Ni-Mn-Ga studies, as the twinning stress for a 10M martensite is estimated to be 1-3 MPa. A similar trend was seen with a bulk thin-plate Ni-Mn-Ga/Hysol 9455 epoxy composite sample (publication III). Tan δ increased with an increasing strain (0 % → 0.7 %) from 0.10 to about 0.27.

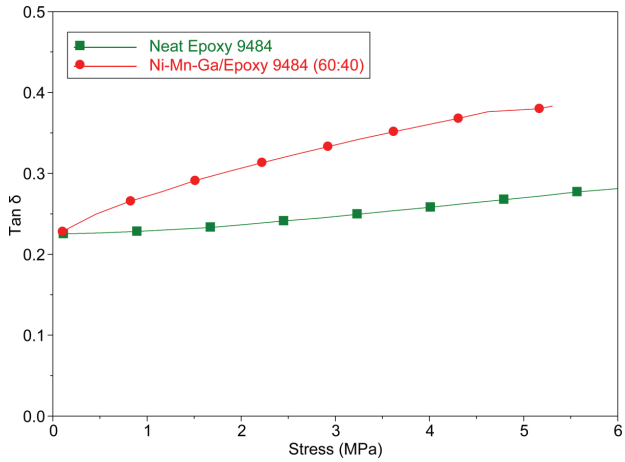

Fig. 6. Damping (tan δ) of a 10M martensite/polymer composite as a function of stress (room temperature, 1 Hz frequency, under 0.31 T magnetic field). Unpublished results

Most actuator designs are targeted to perform at high frequencies, even at hundreds of hertz. Composite samples (epoxy Hysol 9484/10M Ni-Mn-Ga martensite 40/60 vol-%) were tested at 1 Hz and 10 Hz at room temperature, to analyze the influence of a higher frequency on the damping capability. As the damping of 10M martensite depends on twin boundaries and their movements, a higher frequency should result in increased twin boundary movement and higher damping, analogue to increasing stress and strain. The results are shown in Fig. 7. At a frequency of 10 Hz, the composite showed a higher damping capability than at 1 Hz, exactly as expected. Similarly, the bulk Ni-Mn-Ga (unpublished results) showed a higher damping capability at a higher frequency. With high load composites, the mechanical properties and especially the adhesion between the polymer matrix and the Ni-Mn-Ga powder will limit the maximum frequency.

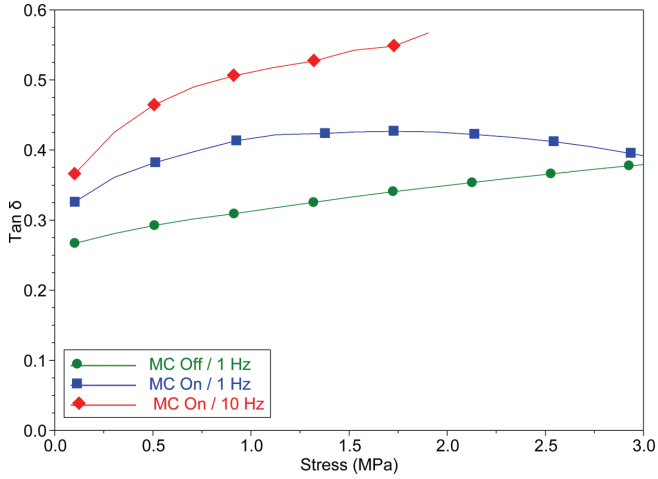

Fig. 7. Damping (tan δ) of a 10M martensite/polymer composite as a function of stress (at room temperature, MC: magnetic circuit). Unpublished results

3.3 CNT/poly(methyl methacrylate) composites with anionic surfactants as dispersing agents [IV]

The dispersion of CNTs into a polymer matrix is a critical factor with carbon nanotube/polymer composites. The CNTs themselves have a very high mechanical strength, for example, the Young's modulus for single-walled carbon nanotubes (SWCNTs) has been calculated to be in the 1 TPa range; for multi-walled carbon nanotubes (MWCNTs), the Young's modulus values are lower, but still very respectable.[49] For typical polymers, the modulus values are only a fraction of these, the Young's modulus for poly(methyl methacrylate), for example, has a value of ~ 2 GPa. The same applies for both electrical and thermal conductivity. In theory, metallic SWCNTs can have electrical conductivities which are more than 1000 times greater than metals such as copper. With MWCNTs and defects in CNTs, the electrical conductivities are lower by one or two orders of magnitude, but the electrical conductivity is still outstanding. The electrical conductivity for PMMA is extremely low.[72-73] Besides electrical conductivity, CNTs have extremely high thermal conductivity. SWCNTs have theoretical thermal conductivities up to ~ 6000 W/mK at room temperature, and the thermal conductivities for MWCNTs are at ~ 3000 W/mK at room temperature.[74] Purely amorphous polymers, such as poly(methyl methacrylate), on the other hand, have a thermal conductivity of ~ 0.1-0.2 W/mK.[75] Without good dispersion of the CNTs, these excellent properties of CNTs cannot be transferred to the composites.

3.3.1 The CNT dispersion and the polymerization of the composites [IV]

Emulsion and suspension polymerization methods are widely used in industry, and composites, manufactured via these methods, can be mass-produced at a reasonable cost.[76] *In situ* polymerization, in the presence of CNTs, is one of the leading methods to produce CNT/polymer composites. The critical factor for CNT dispersion with *in situ* polymerization is the surfactant. With proper surfactant selection, many CNT/polymer composites can be produced, besides in organic solvents, also in an aqueous environment. Surfactants mainly disperse CNTs though hydrophobic/ hydrophilic interactions, where the hydrophobic tail of the surfactant adsorbs on the surface of the CNTs, while the hydrophilic head associates with water for dissolution. The actual surfactant assembly on a CNT surface is not completely clear, but various models, such as (a) cylindrical micelles, (b) hemimicelle, and (c) random adsorption have been proposed. A current understanding of surfactant absorption is that different surfactants seem to behave differently; the diameter of CNT (SWCNT vs. MWCNT) and "kinks" and junctions in the CNT structure also have some influence.[42-43]

In this study, anionic surfactants, sodium dodecyl sulfate, SDS, and a respective derivate with a benzene ring, sodium dodecyl benzene sulfate, DBSA, were used to disperse the CNTs, and to enable the polymerization. SDS and DBSA both have a small molecular size and they adsorb to the surface of the CNTs.

There have been studies made of the optimal surfactant concentration for CNTs, but there are so many variables, such as CNT length and length distribution, CNT diameter and diameter distribution, differences between CNT batches, solvents etc. that no clear conclusions can be drawn from the results.[77-81] For example, small ionic surfactants, such as SDS, have a good dispersion ability for small diameter SWCNTs produced by HiPCO (high-pressure CO conversion synthesis), but for arc-produced SWCNTs, the SDS has a relatively poor dispersion performance. The small ionic surfactants should be used above their cmc (critical micelle concentration) value (SDS: 2.4 mg/mL, water; DBSA: 0.35 mg/mL, water).[82-83] For polymeric surfactants, such as block copolymers, where the dispersion is based on wrapping around the CNT, the cmc dependency has not been so clearly confirmed. The surfactants have a maximum concentration limit; above this, the surfactant itself destabilizes the suspension and the

dispersion capability is reduced. For DBSA, this maximum surfactant concentration is ~ 20 mg/mL.[83]

In this work, 500 mg of anionic surfactant was used for 100 mL of water for both surfactants. The concentration of 5.0 mg/mL for anionic surfactants was in the optimal area. For the monomer feed, a drop by drop method was used i.e. the monomer was slowly added to the reactor. There were two main reasons for this: (1) the amount of surfactant needed by the polymerization could be reduced, and (2) the particle size was reduced. The surfactant concentration has an influence on the polymerization, especially for emulsion polymerization. The higher the surfactant concentration, the higher the total number of polymer particles and the lower the particle size. This, combined with an initial ultrasound treatment while the surfactant was present and finely dispersed into the water, resulted in the small particle size of the latex.[84-93] In this work, this resulted in a nano-scale polymerization, as the amount of finely dispersed surfactant was high. Some polymerization tests were also carried out with a reduced surfactant concentration, which resulted in a higher molecular mass for both polymerization methods, emulsion and combined (unpublished results). On the other hand, the CNT dispersion consumed a significant number of surfactant, so an unknown percentage of surfactant did not participate in the polymerization process leading to a lowered surfactant concentration. Also, the AIBN which was used as the initiator has been reported to react with the surface of the CNTs opening π-bonds, leading to (limited) bonding, and consuming the AIBN and, thus, affecting the molecular weight of the polymer.[94-97] Similar findings were obtained with SEC analysis, as the higher amount of CNTs present in the polymer reduced the soluble part of the composite sample significantly, especially when AIBN was used as the initiator. All these parallel influences make it difficult to estimate the finer relationships between CNT concentration, surfactant concentration, molecular weights, and ultimately, the composite properties.

The quality of the nanodispersion in the composite was difficult to estimate since the electron microscopy had limitations. TEM was used to characterize the morphology, and especially, the CNT dispersion, of the composites. Fig. 7 shows TEM images of composite samples (3.0 wt.% of Nanocyl NC7000 and 3.0 wt.% of Bayer Baytubes). There were no significant aggregates of MWCNTs in the composites. The MWCNT bundles were broken up during the ultrasound treatment and the CNTs were well dispersed into, and isolated within, the polymer matrix. TEM images were also taken from composites based on Nanocyl NC2100 DWCNTs. The

DWCNT dispersion was not as good as the MWCNTs. The DWCNT bundles were "loosened" during the ultrasound treatment, but a complete unbundling was not achieved.

The length of dispersed CNTs was estimated from the TEM images. The average length of Nanocyl NC7000 MWCNTs was ~ 0.5 μm. The length of pristine Nanocyl NC7000 MWCNTs has been estimated to be ~ 0.7 μm by TEM.[98] The length of Bayer Baytubes appeared to be slightly shorter than the Nanocyl NC7000 MWCNTs. Overall, the ultrasound treatment which was required to break up the CNT bundles conserved the CNT length relatively well.

The dispersion quality of CNTs was good for a higher amount of CNTs, showing that the dispersion and polymerization methods were efficient. As can be seen from Fig. 8, the number of CNTs per area was significantly different for thinner Nanocyl NC7000 and thicker Bayer Baytubes. This reflected on composite properties, such as electrical conductivity. Fig. 9 shows a TEM image of a composite with 10 wt.% Nanocyl NC7000. All of the TEM images were taken from DMA test specimens, which had been melt processed after drying the emulsions. Images confirmed that *in situ* polymerization provided a stable dispersion of CNTs, even after thermal processing.

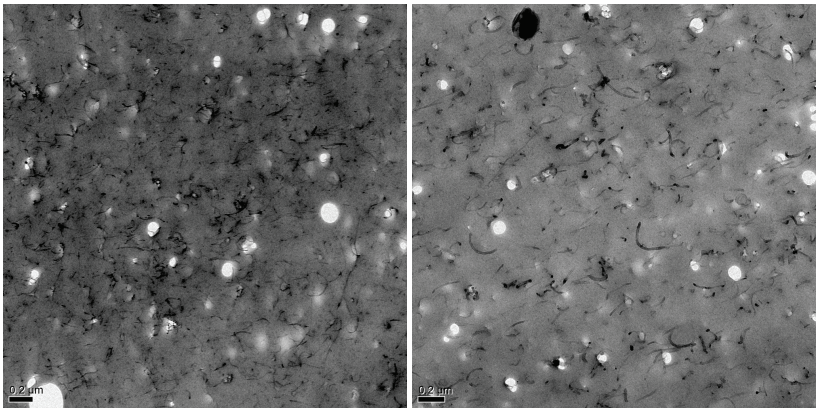

Fig. 8. TEM images of composite samples: (left) KPS, DBSA, 3.0 wt.% MWCNTs (Nanocyl NC7000); (right) KPS, DBSA, 3.0 wt.% MWCNTs (Bayer Baytubes). [IV]

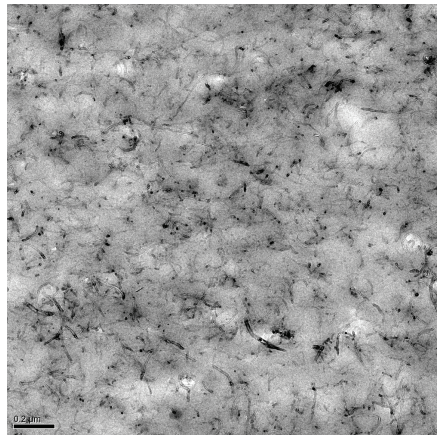

Fig. 9. TEM image of composite sample: KPS, DBSA, 10.0 wt.% MWCNTs (Nanocyl NC7000). Unpublished results

Beside the dispersion of fillers, adhesion between the filler and matrix polymer is crucial for any composite. SEM images were taken to estimate the interface between the polymer and CNTs. Poly(methyl methacrylate) covered the CNTs (both MWCNTs and DWCNTs) during the polymerization, so the polymer wettability to CNTs was at least at the moderate level.

Further evidence of a favourable composite morphology was seen from glass transition temperatures. The glass transition temperature increased up to 20 °C (tan δ peak from DMA) when the MWCNT loading increased from 0 wt.% to 10/15 wt.%; which indicated that the MWCNTs were enhancing the confinement of matrix polymer molecules. The same was seen from the tan δ intensity, which decreased significantly with the increasing CNT content, indicating that fewer polymer chains were able to participate in the glass transition. There was also a greater increase in modulus in the rubbery region than in the glass region, which is typical for nanoscale fillers. Part of the increased T_g resulted from increased molecular weights, since the added CNTs lead to an increased molecular weight, but the major part of the increase in T_g for the composites was caused by the MWCNTs. For DWCNTs, the effect was weaker, as the dispersion of the DWCNTs was not as complete and so the DWCNTs had less surface area.

3.3.2 The mechanical properties of the composites [IV]

Carbon nanotubes can be used to improve the mechanical properties of the polymers, just like macroscopic fillers. But to utilize the nanoscale properties, the dispersion of CNTs and the adhesion between the CNTs and polymer are essential. The low amount of dispersed CNTs act as a reinforcement. However, increasing the nanotube content further causes the modulus values to stabilize or even start to decrease, at some content level. The material will become brittle. This is caused by the agglomeration of the CNTs in the composite.

In this work, the improvements in mechanical properties were limited. The Young's modulus improved, especially when AIBN (combined emulsion/suspension polymerization) was used as an initiator. With non-functionalized MWCNTs, the stress at the break values remained stable or improved slightly up to 6 wt.% of the MWCNTs, when KPS was used as an initiator. With AIBN as an initiator, the stress at the break values started to decrease at a lower MWCNT loading (between 1.5 and 3 wt.%). For mechanical properties, the optimal concentration of Nanocyl NC7000 MWCNTs was ~ 3 wt.%; for thicker Bayer Baytubes MWCNTs, the optimal concentration was higher, over 6 wt.%. The CNTs participated in the polymerization process, which increased the molecular weight as the CNT loading increased. Bayer Baytubes increased the molecular weights significantly more than Nanocyl NC7000 MWCNTs, which was due to the different surface area of MWCNTs. The use of functionalized MWCNTs gave better mechanical properties, especially the stress at break values, than pristine MWCNTs. The reason for the improved mechanical properties was an increased amount of adhesion between the matrix polymer and functionalized CNTs. Overall, thinner MWCNTs (Nanocyl NC7000) improved mechanical properties more than thicker MWCNTs (Bayer Baytubes) with the same CNT loading. Both Nanocyl NC7000 and Bayer Baytubes MWCNTs were short, which limited their capability to improve the mechanical properties. The dispersion of DWCNTs (Nanocyl NC2100) was incomplete, which was, at least, partially responsible for the DWCNT/PMMA composites having slightly lower modulus values than pure PMMA. A summary of the mechanical properties, molecular weights (M_w), and polydispersities (PD) of PMMA/CNT composites is presented in Table 3.

Table 3. A summary of the mechanical properties, molecular weights (M_w), and polydispersities (PD) of CNT/PMMA composites. [IV]

Initiator	CNT loading (wt.%)	CNT treatment	Young's Modulus (MPa)	Stress at break (MPa)	M_w (g/mol)	PD
KPS	-	-	2500	48	144000	3.7
KPS	Baytubes / 3	-	2500	38	152000	2.8
KPS	Baytubes / 6	-	2900	43	504000	2.8
KPS	Baytubes / 15	-	3100	32	661000	2.9
KPS	-	-	2500	49	144000	3.7
KPS	Baytubes / 3	Acid funct.	2900	48	200000	2.6
KPS	Baytubes / 6	Acid funct.	3200	48	229000	3.0
KPS	Baytubes / 15	Acid funct.	3800	41	288000	3.4
KPS	-	-	2500	48	144000	3.7
KPS	NC7000 / 1.5	-	3600	52	155000	2.2
KPS	NC7000 / 3	-	3400	46	145000	2.8
KPS	NC7000 / 6	-	3300	48	160000	3.6
KPS	-	-	2500	48	144000	3.7
KPS	NC7000 / 1.5	Acid funct.	2900	52	175000	3.2
KPS	NC7000 / 3	Acid funct.	2800	53	218000	3.0
KPS	NC7000 / 6	Acid funct.	3200	53	279000	2.8
AIBN	-	-	3400	47	235000	2.3
AIBN	NC7000 / 1.5	-	3300	44	412000	2.4
AIBN	NC7000 / 3	-	3400	27	486000	2.3
AIBN	NC7000 / 6	-	4000	30	395000	2.5
AIBN	-	-	3400	47	235000	2.3
AIBN	NC2100 / 1.5	-	3300	44	240000	2.5
AIBN	NC2100 / 3	-	3000	51	281000	2.8

3.3.3 The electrical conductivity of the composites [IV]

Improved electrical conductivity is perhaps the most promising property of composite applications for CNTs at the moment. If CNTs are efficiently dispersed and yet percolate through a matrix, a very small amount (even 0.1 wt.%) of CNTs can confer good electrical conductivity on otherwise insulating polymers. The percolation threshold is higher for MWCNTs than for SWCNTs. The percolation threshold depends on many factors, like the matrix polymer, the processing of the composite, CNT production method, CNT conductivity, and CNT length.[99-103] CNT length is a critical factor, as the resistance of CNTs is practically completely junction controlled, as a defect-free tube itself is ballistically conductive. The values for junction resistances are only estimates, but very high values, such as 10^{13} Ω have been calculated via Monte Carlo simulations.[104-105] The more CNTs the electron must pass through to travel a certain distance, the higher the resistance will be. For polymeric composites, the maximum tunneling distance has been calculated to be ~ 1.8 nm. If the distance between two

CNTs is more than that, the resistance is rapidly increasing. In short, this means that long CNTs, with an effective dispersion, are required for a low percolation threshold.[106]

Three different CNTs (Bayer Baytubes, MWCNT; Nanocyl NC7000; MWCNT; and Nanocyl NC2100, DWCNT) were used to estimate the electrical conductivity of the composites. The initiator/polymerization method affected the electrical conductivity significantly; the use of AIBN as an initiator gave better electrical conductivities for the composites. The electrical conductivities for poly(methyl methacrylate) based composites are shown in Fig. 10. Based on TEM images, the composites with AIBN as an initiator had a weak "chain-like" orientation, while the composites with KPS as an initiator were randomly oriented. The different initiators created different morphologies, and even a slight orientation of CNTs can affect the percolation threshold. For composites with NC7000 MWCNTs, the percolation threshold was ~ 1.5 wt.% MWCNTs. With Bayer Baytubes, the percolation threshold shifted to 3 – 6 wt.% MWCNTs. This was caused by the difference in the CNT diameter, leading to a lower number of Bayer Baytubes, compared to Nanocyl NC7000 in the same sample volume. Tests were also conducted with acid functionalized MWCNTs. The electrical conductivity was better for composites with non-functionalized MWCNTs, which indicated that the acid functionalization process either caused some damage to the CNTs or shortened them. The conductivity of NC2100 (DWCNTs)-based composites was rather poor (comparable to Nanocyl NC7000 MWCNTs); this was related to the rather poor dispersion of the DWCNTs, which was seen in the TEM images.

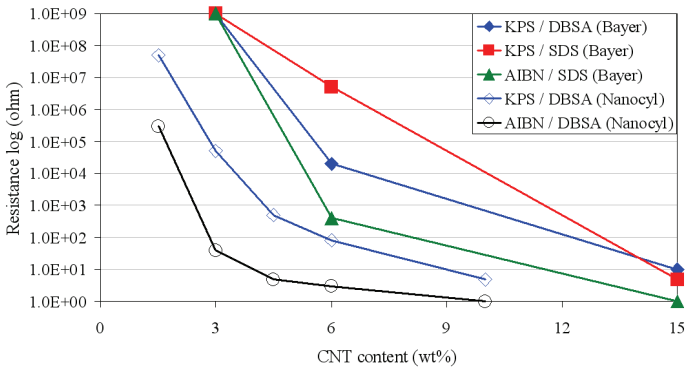

Fig. 10. Electrical (surface) conductivities for MWCNT/PMMA composites. [IV]

3.3.4 The thermal conductivity of the composites [IV]

The transport of thermal energy in CNTs is related to a phonon conduction mechanism, which is dominated by scattering effects such as interfacial boundary and defect scattering. A high aspect ratio of particles is preferred, as the phonons can transfer over a long distance without any particle-particle transition. If the CNTs are defect-free, the defect scattering will be minimal, leading to better thermal conductivity. CNT functionalization, which is often carried out for better mechanical properties, is not preferred, as it causes damage to the outer CNT layer and therefore increases scattering. Mathematical theories, and practical research, predict that the bulk of the heat flow through the CNTs is carried by the outer layers of MWCNTs, while the contribution of inner layers is small. This is one factor that provides a smaller value of the effective conductivity than expected. It has been speculated that thick MWCNTs, with a high aspect ratio, should be most favorable for the enhancement of the thermal conductivity of polymer composites. They have a smaller surface area, and thus, lower interfacial boundary surface scattering and matrix coupling. Additionally, internal layers are available for phonon conduction with a minimal loss due to a negligible scattering with the matrix. One significant factor on the thermal conductivity of the CNT/polymer composites is the crystallinity of the polymer. A high crystallinity of the polymer reduces the interfacial thermal resistance, by providing more "bridges" between CNTs, thus, leading to higher thermal conductivity.[74, 107-109]

Thermal conductivity for neat poly(methyl methacrylate) samples were measured with Hotdisk method, and was estimated to be ~ 0.19-0.21 W/mK. These values are ~ 1/10,000 of typical MWCNT thermal conductivity. The thermal conductivities for composites are shown in Fig. 11. When thin Nanocyl NC7000 MWCNTs were added to the PMMA matrix, the thermal conductivity increased by about 70% (6 wt.% load), and then stabilized. With Bayer Baytubes, the thermal conductivity steadily increased with MWCNT loading, up to 15 wt.% Baytubes. The thermal conductivities of Nanocyl 2100 DWCNT/PMMA composites were also tested, and they were found to improve thermal conductivity like thin Nanocyl NC7000 MWCNTs (up to 3.0 wt.%).

The thermal conductivity of polymers can be improved by CNTs, but the improvement in the overall conductivity is negligible for amorphous polymers such as poly(methyl methacrylate). The *in situ* polymerization method, where the polymer forms layers around the CNTs during

polymerization, is not the optimal production method to obtain good thermal conductivity. The heat cannot be transferred effectively, as the CNTs are isolated in the polymer matrix and are not physically connected with each other. This, combined with short length of CNTs, resulted in limited improvements in thermal conductivity. Thicker MWCNTs had better thermal conductivity at high CNT loading; the initiator selection (KPS or AIBN) did not have a significant impact on the thermal conductivity. The surfactant, on the other hand, had an influence on the thermal conductivity, since the composites polymerized with SDS as the surfactant had a higher thermal conductivity, at least for Bayer Baytubes. There is probably a difference in composite morphology between DBSA and SDS which explains the results, but dispersion studies from TEM images did not provide support for these observations, as all dispersions appeared to be similar.

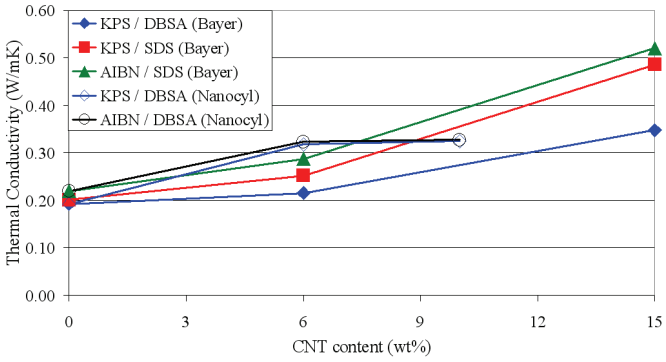

Fig. 11. The thermal conductivities for MWCNT/PMMA composites. [IV]

3.4 CNT/poly(methyl methacrylate) composites with cationic stearyl methacrylate copolymers as dispersing agents [V]

Most *in situ* polymerizations in the presence of CNTs have been carried out with ionic surfactants. As the control of polymerization methods has been improved over the last couple of decades and new polymer structures have been introduced; new potential dispersing agents have been introduced. The most interesting of these new surfactants for CNT/polymer composites are conjugated polymers and block copolymers in particular. Block copolymers consist of two or more chemically distinct polymer chains, leading to a phase separation. As the blocks are linked with covalent bonds, their phase separation is limited, enabling sub-micron self-assembly. With

CNTs, attempts have been made by block copolymers to disperse the CNTs into solvent or to graft the block copolymers directly into CNTs. With CNTs grafted into block copolymers, the CNTs could be assembled into a defined order.[110-112] A more common use for block copolymers with CNTs is as a surfactant to disperse the CNTs into a suitable solvent. The solvent has an important function with block copolymers: the insoluble block will minimize the contact with a solvent, and on the other hand, the soluble block orientates in the solvent.[113-114] If water is used as the solvent, an amphiphilic copolymer with a long hydrocarbon segment combined with some strongly hydrophilic segment would be a good candidate as a dispersing agent.

3.4.1 CNT dispersion on the composites [V]

In this part of the study, amphiphilic copolymers (poly[(stearyl methacrylate)-*stat*-([2-(methacryloyloxy)ethyl] trimethyl ammonium iodide)]) were used as dispersing agent to produce composites using an *in situ* emulsion/suspension polymerization method and water as the solvent. Three different polymers were used as surfactants to disperse the MWCNTs, and to form a composite. Two of these were cationic stearyl methacrylate (SMA) copolymers, with 13 and 17 mol-% of SMA. The third one was quaternized poly[2-(dimethylamino)ethyl methacrylate] (PDM) homopolymer, which was used as a reference.

The effective dispersion of CNTs, using anionic surfactants, required a high amount of surfactant, which remained in the composite after processing steps (publication IV). With amphiphilic SMA copolymers, a relatively similar structure than the poly(methyl methacrylate) matrix was used to provide compatibility between the surfactant and polymer. Also, if a lower amount of amphiphilic copolymers could be used, the composite properties might be improved as the influence of the surfactant could be reduced.

At first, the dispersion capability of amphiphilic copolymers for MWCNTs in water was tested. With amphiphilic copolymers, the initial ultrasound treatment dispersed the MWCNTs visually uniformly into the water; the result was a completely black mixture with no significant re-agglomeration after one week. After 30 days, some re-agglomeration had occurred, but overall, the stability of the dispersion with SMA copolymers was good. The dispersion of MWCNTs with quaternized homopolymer (PDMQ) was

significantly worse, with severe re-agglomeration already seen after one week.

Transmission electron microscopy was used to characterize the morphology and MWCNT dispersion of the composites. Fig. 12 shows typical TEM images of composites (6.0 wt.% Nanocyl NC7000) with cationic SMA copolymers. The MWCNTs were well dispersed into the polymer matrix. There was no noticeable difference in dispersion quality between the PSMA13Q and PSMA17Q amphiphilic copolymers, nor between the amounts of 125 mg and 250 mg; all showed good dispersion, based on TEM. However, when compared to the dispersion of CNTs with anionic surfactants, the dispersions were not as even. Although no significant re-aggregates of CNTs could be seen, the quality of dispersions were more varied. The dispersion of MWCNTs with PDMQ was very poor. The thickness of the MWCNTs in the composites was in the range of 10 nm, which indicated that the MWCNTs were either individually dispersed or consisted of bundles with very low numbers of MWCNTs. This further indicated that the cationic amphiphilic copolymers were able to prevent the MWCNTs from re-agglomerating during the polymerization. At 3.0 wt.% MWCNT, the MWCNTs were mainly separated from each other by polymer, which limited the electrical conductivity. At 6.0 wt.% MWCNT, the number of MWCNTs was high enough that the MWCNTs began to overlap each other.

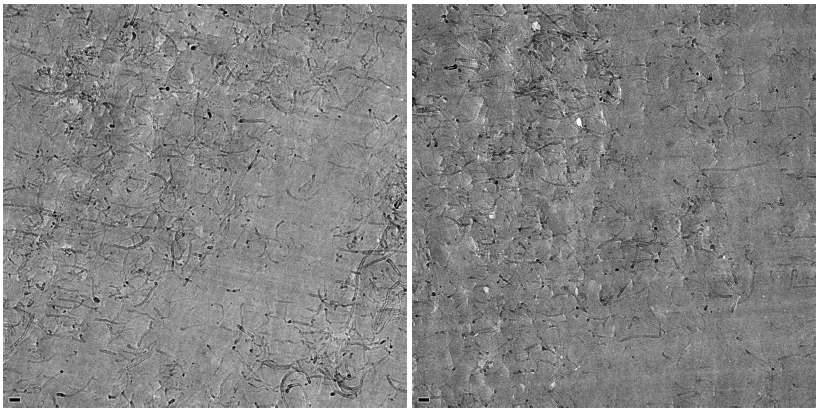

Fig. 12. TEM images of composite samples: (left) PSMA13Q, 6.0 wt.% Nanocyl NC7000; (right) PSMA17Q, 6.0 wt.% Nanocyl NC7000 [V]

3.4.2 The mechanical and conductive properties of the composites [V]

The use of amphiphilic copolymers as surfactants only had a minor influence on the molecular weight, unlike with the anionic surfactants. The changes in the mechanical properties of the composites were induced by the added MWCNTs.

A summary of the mechanical properties, molecular weights (M_w), and polydispersities (PD) of the composites is shown in Table 4. With amphiphilic copolymers the influence of a surfactant concentration on the properties of composites was measured thoroughly. When 250 mg of an amphiphilic copolymer was used as a surfactant, the Young's modulus increased slightly. For PSMA13Q, the stress at break values increased with CNT loading, but for PSMA17Q, a decrease was seen at a higher CNT loading. When 125 mg of PSMA13Q or PSMA17Q was used as a surfactant, the Young's modulus values were comparable to those which were obtained using 250 mg of surfactant, but the stress at the break values remained high, even at a high CNT loading (6 wt.%). 500 mg of amphiphilic copolymers was also tested, but the results were negative for mechanical properties. Based on these results, the lowest amount (125 mg) of amphiphilic copolymer was the optimal amount of surfactant, for the mechanical properties of the composites. If more copolymer was present, the mechanical properties began to decrease. This was possibly due to the formation of a copolymer-rich phase, thus, affecting the contact between MWCNTs and PMMA matrix. The pure PDMQ worked adequately at low MWCNT loadings (up to ~ 3.0 wt.%), but at 6.0 wt.%, the modulus values of the composite decreased by over 50% and the stress at break values even more. The obvious reason for this is that the cationic homopolymer was not able to disperse the increasing loading of MWCNTs and severe agglomeration occurred, thus decreasing the mechanical properties.

Table 4. A summary of the mechanical properties, molecular weights (M_w), and polydispersities (PD) of the composites. [V]

Surfactant	Amount of surfactant (mg)	CNT loading (wt.%)	Young's Modulus (MPa)	Stress at break (MPa)	M_w (g/mol)	PD
PSMA13Q	250	-	3900	42	452000	2.2
PSMA13Q	250	NC7000 / 1.5	4000	46	439000	3.3
PSMA13Q	250	NC7000 / 3	4200	55	403000	2.6
PSMA13Q	250	NC7000 / 6	4400	47	478000	2.2
PSMA13Q	125	-	3500	38	719000	2.8
PSMA13Q	125	NC7000 / 1.5	3700	44	482000	3.5
PSMA13Q	125	NC7000 / 3	3900	42	500000	2.8
PSMA13Q	125	NC7000 / 6	4200	47	533000	1.7
PSMA13Q	125	NC7000 / 6	4200	47	533000	1.7
PSMA13Q	250	NC7000 / 6	4400	47	478000	2.2
PSMA13Q	500	NC7000 / 6	4300	25	512000	2.2
PSMA17Q	250	-	3800	52	577000	1.7
PSMA17Q	250	NC7000 / 1.5	4000	51	446000	3.1
PSMA17Q	250	NC7000 / 3	4100	31	488000	2.4
PSMA17Q	250	NC7000 / 6	4400	35	585000	2.3
PSMA17Q	125	-	3200	52	493000	3.9
PSMA17Q	125	NC7000 / 1.5	3700	46	551000	4.2
PSMA17Q	125	NC7000 / 3	3800	53	582000	2.8
PSMA17Q	125	NC7000 / 6	4400	49	700000	2.4
PSMA17Q	125	NC7000 / 6	4400	49	700000	2.4
PSMA17Q	250	NC7000 / 6	4400	35	585000	2.3
PSMA17Q	500	NC7000 / 6	3300	32	564000	2.6
PDMQ	250	-	3500	47	409000	2.8
PDMQ	250	NC7000 / 1.5	3600	44	386000	3.8
PDMQ	250	NC7000 / 3	3700	46	412000	2.8
PDMQ	250	NC7000 / 6	1900	18	545000	2.9

The glass transition temperatures (T_g) for composites with cationic SMA copolymers as dispersants were also measured. The glass transition temperature increased by 3-4 °C (tan δ peak from DMA) when MWCNT loading increased from 0 wt.% to 6 wt.%, indicating that the MWCNTs had some interaction with the matrix polymer molecules, thus, limiting the movement of polymer chains. The increasing T_g suggested that the dispersion of MWCNTs was relatively good, as poor CNT dispersion may actually decrease the T_g by generating more free volume in the matrix. Tan δ curves showed only one peak, without any noticeable shoulders or broadenings, which suggested that the polymer chains in the composites were relatively uniform; meaning that the molecular weights of neat polymer and polymer possibly grafted with MWCNTs were about the same. The intensity of tan δ peaks also decreased with increased MWCNT loading, which indicated that fewer polymer chains were participating in the T_g transition.

The surface electrical conductivities for composites with an amphiphilic copolymer as the surfactant were measured (Fig. 13). Two cationic copolymers with different percentages of SMA (PSMA13Q (13 mol-% of SMA) and PSMA17Q (17 mol-% of SMA)) were tested. The electrical conductivity was better with a lower amount of surfactant (125 mg). A possible explanation was the higher coverage of CNTs with the cationic copolymer (or homopolymer, PDMQ) in the composite structure, meaning that there was a widening barrier for the electrons to cross as the surfactant concentration increased. Overall, the percolation threshold with cationic copolymers was higher than with anionic surfactants. The main reason was a more uneven CNT dispersion than with anionic surfactants, which was seen with TEM. The percolation threshold with cationic copolymers was 3.0 – 4.0 wt.% MWCNTs. With a more optimized concentration of an amphiphilic copolymer, the percolation threshold could probably be lowered.

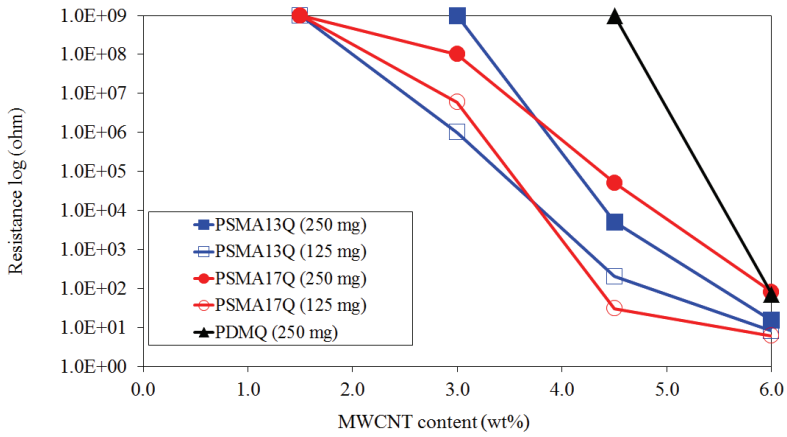

Fig. 13. Electrical (surface) conductivities for MWCNT/PMMA composites. [V]

As with composites using anionic surfactants, thermal conductivities were measured using a Hot Disk Thermal Constants Analyzer. At low MWCNT loadings (up to 4.5 wt.%), the thermal conductivity was about the same for both concentrations of cationic copolymer (125 mg and 250 mg). At high loading (6.0 wt.%), the thermal conductivity was better with the higher concentration of amphiphilic copolymer, which was the opposite to what was observed for electrical conductivity. The PSMA17Q (17 mol% of SMA) provided higher thermal conductivities than PSMA13Q, especially at higher MWCNT loading, which might correspond to having a slightly better dispersion and a different orientation capability at the higher SMA content.

The PDMQ could not disperse the MWCNTs properly, leading to a composite with agglomerated MWCNTs in the polymer matrix. With cationic copolymers, the thermal conductivity increased by up to 110% (6 wt.% load), which was a relatively higher increase than with anionic surfactants.

3.5 CNT/poly(methyl methacrylate) composites as masterbatches [VI]

The direct melt mixing of carbon nanotubes into polymers, using extrusion, has attracted significant interest after the discovery of CNTs. Extrusion is a widely used method, which is both inexpensive and suitable for a wide variety of polymers. The challenge with extrusion based CNT/polymer composites are insufficient shear forces. The energy released during extrusion process cannot break up CNT bundles and disperse CNTs uniformly, in so far as the interaction between CNTs and the polymer matrix is not strong enough.[115-117] With proper CNT functionalization, the interaction can be enhanced, leading to improved dispersion and composite properties, but CNT functionalization induces higher production costs. To solve or at least to diminish these challenges, masterbatches containing 10-20 wt.% of CNTs, can be used as a CNT source. Most commercial masterbatches are polypropylene (PP) based, as the dispersion of CNTs into non-polar polymers is especially difficult to achieve due to filler-matrix incompatibility. The masterbatch is simply diluted into a matrix polymer via extrusion. The CNT dispersion via a masterbatch approach is usually better than with the direct melt mixing of CNTs and a polymer, but not at the level that can be achieved via *in situ* polymerization. The extrusion procedure cannot disperse the CNTs invidually into the matrix. The masterbatch containing the CNTs is divided into domains located in the matrix. A continuous phase must be formed before the percolation can be achieved. The quality of the mixing process is determined by the viscosities of the matrix and the masterbatch and by the shear rate.[118-122]

In this study, *in situ* polymerized poly(methyl methacrylate) composites containing 10 wt.% of Nanocyl NC7000 MWCNTs were used as a masterbatch. With *in situ* polymerization, the composite viscosity can be tailored, based on the desired viscosity to enable efficient mixing.

The direct melt mixing of Nanocyl NC7000 MWCNTs with commercial PMMA was carried out, but the composites were not conductive, even at 4

wt.% MWCNTs. This was due to an incompatibility between PMMA and CNTs, the interaction between these was weak and the MWCNTs remained agglomerated. With a PMMA masterbatch, the percolation threshold was below 4 wt.%. To measure the viscosity of the composites, rheological studies were carried out. The *in situ* polymerized masterbatch, containing 10 wt.% of MWCNTs, had a high viscosity when compared to the matrix polymer, thus, preventing the effective mixing in the melt mixer. Glycerol was used as a plastizer to lower the viscosity of the masterbatch. When the viscosity of the PMMA-masterbatch was decreased with glycerol, the percolation threshold was below 3 wt.% CNTs. Moderate conductivity was achieved with 2 wt.% CNTs, when a higher amount of glycerol was added to the PMMA-masterbatch. *In situ* polymerization can be used to produce composites with high enough CNT content that they can be used as masterbatches. The viscosity has to be suitable to ensure the blending of the masterbatch and matrix; otherwise, the dispersion of CNTs via melt mixing will not be efficient.

Besides the percolation threshold studies, the mechanical properties of the composites were measured. The melt mixing of Nanocyl NC7000 MWCNTs directly with commercial PMMA decreased the mechanical properties. The tensile modulus was mainly affected by the plasticizer and not by MWCNTs. On the other hand, the tensile strength of PMMA composites decreased after the addition of MWCNTs, and the decrease was more pronounced with the use of a PMMA-masterbatch than with pure MWCNTs. The tensile strength of the composites was higher when a plasticizer was added to the masterbatch.

4. CONCLUSIONS

Ni-Mn-Ga is a metal alloy, which has an exceptionally large shape change under a magnetic field or external stress. A number of Ni-Mn-Ga bulk studies were carried out using dynamic mechanical analysis. DMA testing showed a strong temperature dependency for damping, the peak of the damping occurred at the martensitic transformation. 10M martensite had the highest damping values, but the damping decreased relatively more at a lower temperature than with a non-modulated or mixed martensite. The decreasing storage modulus with an increasing temperature correlated with an increasing damping as the mobility of twin boundaries was increasing with an increasing temperature at the martensite region. The stress dependency on the damping was measured for a non-modulated martensite. Increasing stress led to modulus softening and easier movement for the twins, thus leading to increasing damping. This indicated a twin boundary motion, which is the main contribution for damping in non-modulated martensites. DMA proved to be a very suitable method for damping studies with bulk Ni-Mn-Ga, as several variables such as modulus, damping, and frequency could be obtained with a single run over a temperature range.

Ni-Mn-Ga/epoxy composites were manufactured using Ni-Mn-Ga as powder, ribbons, and thin bulk. Enhanced damping was found in composites with polymer stiffness near to Ni-Mn-Ga. With a too hard matrix material, the Ni-Mn-Ga insert remained constrained without any possibility to deform. With a too soft matrix polymer, the damping energy could not be transferred effectively. A magnetic circuit was designed and built for a DMA system to measure the active damping of Ni-Mn-Ga/polymer composites under a magnetic field. Composites were manufactured under the magnetic field so that the Ni-Mn-Ga powder could be orientated in the composite. Damping was improved, both under the magnetic field and with Ni-Mn-Ga orientation. Studies of Ni-Mn-Ga bulk and Ni-Mn-Ga/polymer composites showed that numerous factors have an influence on composite designs with Ni-Mn-Ga and that designing an active high frequency damping composite with a wide enough temperature window is and will be a challenge.

In addition to the studies with bulk Ni-Mn-Ga and Ni-Mn-Ga/polymer composites, carbon nanotube/poly(methyl methacrylate) nanocomposites

were prepared via *in situ* polymerization. Two types of dispersing agents, anionic surfactants and amphiphilic copolymers were used to disperse the CNTs. The dispersion of MWCNTs into the PMMA matrix was efficient for both types of surfactants, but slightly more uniform dispersion was formed with anionic surfactants. High MWCNT loadings (up to 10 wt.%) could be dispersed into the PMMA matrix. Especially with anionic surfactants, the carbon nanotubes participated on polymerization and, thus, affected the molecular weight of the PMMA. The mechanical properties of composites were improved, but the improvements were rather limited for both types of dispersing agents. The percolation threshold was lower with anionic surfactants, which was related to a better CNT dispersion. The thermal conductivity of CNT/PMMA composites was measured. The improvement in thermal conductivity was more pronounced when amphiphilic copolymers were used as dispersing agents. Opposite to electrical conductivity, thicker Bayer Baytubes improved the thermal conductivity more than thin MWCNTs.

Finally, high loading CNT/PMMA composites were used as a masterbatch and diluted into commercial PMMA by melt mixing, and compared to composites prepared by the direct melt mixing of CNTs and polymer matrix. There was no significant difference in mechanical properties between the masterbatch-approach and the direct melt mixing. The percolation threshold for electrical conductivity, on the other hand, was lower with the masterbatch-approach, when the viscosities of the CNT/PMMA composite and PMMA matrix were comparable.

For the Ni-Mn-Ga/polymer composites the objective for future research would be to combine the learned aspects like requirements for polymer matrix, Ni-Mn-Ga magnetic orientating, and compression of Ni-Mn-Ga material with quality Ni-Mn-Ga powder to create a working composite for controlled active damping and energy harvesting. The particle size and particle size distribution, including the shape of the particles, for Ni-Mn-Ga powder should also be investigated to find the optimal parameters. For the CNT/polymer composites, a composite with good CNT dispersion using longer MWCNTs, or SWCNTs, would be the essential objective. The dispersion of longer CNTs into polymer matrix is more difficult than with short CNTs but the mechanical properties and especially electrical conductivity would be improved. Another research goal would be to optimize the structure of amphiphilic copolymers used in publication V for CNT dispersion. Also, the optimal amount of amphiphilic copolymers for effective CNT dispersion should be investigated.

REFERENCES

1. Bhattacharya, S.N., Gupta, R.K., Kamal, M.R. (Eds.), *Polymeric nanocomposites: theory and practice*, Carl Hanser Verlag, Munich, Germany 2008, 383 p.

2. Advani, S.G. (Ed.), *Processing and properties of nanocomposites*, World Scientific Publishing Co. Pte. Ltd., Singapore, Singapore 2007, 450 p.

3. Ahir, S.V., Huang, Y.Y., Terentjev, E.M., Polymers with aligned carbon nanotubes: active composite materials, *Polymer* **49** (2008) 3841-3854.

4. O´Handley, R.C., Allen, S.M., Shape-memory alloys, magnetically activated ferromagnetic shape-memory materials. In *Encyclopedia of Smart materials*, Edit. M. Schwartz, John Wiley & Sons, New York 2002, pp. 936-951.

5. Aaltio, I., Heczko, O., Söderberg, O., Hannula, S.-P., Shape-memory alloys and effects: Types, functions, modeling, and applications. In *Smart materials*, Edit. M. Schwartz, CRC Press, Boca Raton 2009, pp. 20/1-8.

6. Söderberg, O., Aaltio, I., Ge, Y., Heczko, O., Hannula, S.-P., Ni-Mn-Ga multifunctional compounds, *Mater. Sci. Eng. A* **481-482** (2008) 80-85.

7. Söderberg, O., Aaltio, I., Ge, Y., Liu, X., Hannula, S.-P., Recent developments of magnetic SMA, *Adv. Sci. Tech.* **59** (2008) 1-10.

8. Dunand, D.C., Müllner, P., Size effects on magnetic actuation in Ni-Mn-Ga shape-memory alloys, *Adv. Mater.* **23** (2011) 216-232.

9. Han, M., Bennett, J.C., Gharghouri, M.A., Chen, J., Hyatt, C.V., Mailman, N., Microstructure characterization of the non-modulated martensite in Ni-Mn-Ga alloy, *Mater. Charact.* **59** (2008) 764-768.

10. Sozinov, A., Likhachev, A.A., Ullakko, K., Crystal structures and magnetic anisotropy properties of Ni-Mn-Ga martensitic phases with giant magnetic-field-induced strain, *IEEE Trans. Magn.* **38** (2002) 2814-2816.

11. Pons, J., Santamarta, R., Chernenko, V.A., Cesari, E., Structure of the layered martensitic phases of Ni-Mn-Ga alloys, *Mater. Eng. A* **438-440** (2006) 931-934.

12. Richard, M.L., Feuchtwanger, J., Allen, S.M., O´Handley, R.C., Lázpita, P., Barandiaran, J.M., Martensite transformation in Ni-Mn-Ga ferromagnetic shape-memory-alloys, *Metall. Mater. Trans. A* **38** (2007) 777-780.

13. Straka, L., Heczko, O., Novák, V., Lanska, N., Study of austenite-martensite transformation in Ni-Mn-Ga magnetic shape memory alloy, *J. Phys. IV* **112** (2003) 911-915.

14. Aaltio, I., Söderberg, O., Ge, Y., Hannula, S.-P., Twin boundary nucleation and motion in Ni-Mn-Ga magnetic shape memory material with a low twinning stress, *Scripta Mater.* **62** (2010) 9-12.

15. Straka, L., Heczko, O., Hänninen, H., Activation of magnetic shape memory effect in Ni-Mn-Ga alloys by mechanical and magnetic treatment, *Acta Mater.* **56** (2008) 5492-5499.

16. Ge, Y., Jiang, H., Sozinov, A., Söderberg, O., Lanska, N., Keränen, J., Kauppinen, E.I., Lindroos, V.K., Hannula, S.-P., Crystal structure and microtwin interface of five-layered martensite in Ni-Mn-Ga magnetic shape memory alloy, *Mater. Sci. Eng. A* **438-440** (2006) 961-964.

17. Han. M., Bennett, J.C., Charghouri, M.A., Chen, J., Hyatt, C.V., Understanding modulated twin transition at the atomic level, *Acta Mater.* **55** (2007) 1731-1740.

18. Likhachev, A.A., Sozinov, A., Ullakko, K., Different modeling concepts of magnetic shape memory and their comparison with some experimental results obtained in Ni-Mn-Ga, *Mater. Sci. Eng. A* **378** (2004) 513-518.

19. Han, M., Kong, F.F., Twin boundary structure of the modulated variants in a Ni-Mn-Ga alloy, *J. Alloys Compd.* **458** (2008) 218-222.

20. Heczko, O, L'vov, V.A., Straka, L., Hannula, S.-P., Magnetic indication of the stress-induced martensitic transformation in ferromagnetic Ni-Mn-Ga alloy, *J. Magn. Magn. Mater.* **302** (2006) 387-390.

21. Söderberg, O., Straka, L., Novak, V., Heczko, O., Hannula, S.-P., Lindroos, V.K., Tensile/compressive behaviour of non-layered tetragonal $Ni_{52.8}Mn_{25.7}Ga_{21.5}$ alloy, *Mater. Sci. Eng. A* **386** (2004) 27-33.

22. Chmielus, M., Rolfs, K., Wimpory, R., Reimers, W., Müllner, P., Schneider, R., Effects of surface roughness and training on the twinning stress of Ni-Mn-Ga single crystals, *Acta Mater.* **58** (2010) 3952-3962.

23. Morawiec, H., Goryczka, T., Lelatko, J., Prusik, K., Drdzén, A., Effect of deformation on structure and mechanical behavior of polycrystalline Ni-Mn-Ga alloys, *Eur. Phys. J. Special Topics* **158** (2008) 93-98.

24. Dubowik, J., Kudryavtsev, Y.V., Lee, Y.P., Martensitic transformation in Ni_2MnGa films: a ferromagnetic resonance study, *J. Appl. Phys.* **95** (2004) 2912-2917.

25. Suorsa, I., Tellinen, J., Ullakko, K., Pagounis, E., Voltage generation induced by mechanical straining in magnetic shape memory materials, *J. Appl. Phys.* **95** (2004) 8054-8058.

26. Humbeeck, J.V., Kustov, S., Active and passive damping of noise and vibrations through shape memory alloys: applications and mechanism, *Smart Mater. Struct.* **14** (2005) S171-S185.

27. Hornbogen, E., Comparison of shape memory metals and polymers, *Adv. Eng. Mater.* **8** (2006) 101-106.

28. Feuchtwanger, J., Michael, S., Juang, J., Bono, D., O´Handley, R.C., Allen, S.M., Jenkins, C., Energy absorption in Ni-Mn-Ga-polymer composites, *J. Appl. Phys.* **93** (2003) 8528-8530.

29. Ham-Su, R., Healey, J.P., Underhill, R.S., Farrell, S.P., Cheng, L.M., Hyatt, C.V., Rogge, R., Gharghouri, M.A., Fabrication of magnetic shape memory alloy/polymer composites. In *Smart Structures and Materials 2005: Active Materials: Behavior and Mechanics: 5761 (Proceedings of SPIE)*, Edit. W.D. Armstrong, SPIE, Bellingham 2005, pp. 490-500.

30. Feuchtwanger, J., Richard, M.L., Large energy absorption in Ni-Mn-Ga/polymer composites, *J. Appl. Phys.* **97** (2005) 10M319/1-3.

31. Feuchtwanger, J., Griffin, K., Huang, J., Bono, D., O´Handley, R.C., Allen, S.M., Mechanical energy absorption in Ni-Mn-Ga polymer composites, *J. Magn. Magn. Mater.* **272-276** (2004) 2038-2039.

32. Hosada, H., Takeuchi, S., Inamura, T., Wakashima, K., Material design and shape memory properties of smart composites composed of polymer and ferromagnetic shape memory alloy particles, *Sci. Tech. Adv. Mater.* **5** (2004) 503-509.

33. Tian, B., Chen, F., Tong, Y.X., Li, L., Zheng, Y.F., Bending properties of epoxy resin matrix composites filled with Ni-Mn-Ga ferromagnetic shape memory alloy powders, *Mater. Lett.* **63** (2009) 1729-2732.

34. Sun, X., Xie, C., Damping characteristics of a NiMnGa/polymer composite material, *Mater. Sci. Forum* **561-565** (2007) 697-699.

35. Okuno, M., Inamura, T., Kanetaka, H., Hosada, H., Compression behavior and texture development of polymer matrix composites on NiMnGa ferromagnetic shape memory alloy particles, *Mater. Sci. Forum* **654-656** (2010) 2103-2106.

36. Zeng, M., Or, S.W., Chan, H.L.W., Large magnetoelectric effect from mechanically mediated magnetic field-induced strain effect in Ni-Mn-Ga single crystal and piezoelectric effect in PVDF polymer, *J. Alloys Compd.* **490** (2010) L5-L8.

37. Boonyongmaneerat, Y., Chmielus, M., Dunand, D.C., Müllner, P., Increasing magnetoplasticity in polycrystalline Ni-Mn-Ga by reducing internal constraints through porosity, *Phys. Rev. Lett.* **99** (2007) 247201/1-4.

38. Nessim, G.D., Properties, synthesis, and growth mechanisms of carbon nanotubes with special focus on thermal chemical vapor deposition, *Nanoscale* **2** (2010) 1306-1323.

39. Graham, A.P., Duesberg, G.S., Hoenlein, W., Kreupl, F., Liebau, M., Martin, R., Rajasekharan, B., Pamler, W., Seidel, R., Steinhoegl, W., Unger, W., How do carbon nanotubes fit into the semiconductor roadmap?, *Appl. Phys. A* **80** (2005) 1141-1151.

40. Grady, B.P., Recent developments concerning the dispersion of carbon nanotubes in polymers, *Macromol. Rapid Commun.* **31** (2010) 247-257.

41. Ma, P.-C., Siddiqui, N.A., Marom, G., Kim, J.K., Dispersion and functionalization of carbon nanotubes for polymer-based nanocomposites: a review, *Compos. Part A* **41** (2010) 1345–1367.

42. Wang, H., Dispersing carbon nanotubes using surfactants, *Curr. Opin. Colloid Interface Sci.* **14** (2009) 364-371.

43. Tummala, N.R., Striolo, A., SDS surfactants on carbon nanotubes: aggregate morphology, *ACS Nano* **3** (2009) 595-602.

44. Moore, V.C., Strano, M.S., Haroz, E.H., Hauge, R.H., Smalley, R.E., Invidually suspended single-walled carbon nanotubes in various surfactants, *Nano Lett.* **3** (2003) 1379-1382.

45. Cotiuga, I., Picchioni, F., Agarwal, U.S., Wouters, D., Loos, J., Lemstra, P.J., Block-copolymer-assisted solubilization of carbon nanotubes and exfoliation monitoring through viscosity, *Macromol. Rapid Commun.* **27** (2006) 1073-1078.

46. Mountrichas, G., Tagmatarchis, N., Pispas, S., Synthesis and solution behavior of carbon nanotubes decorated with amphiphilic block polyelectrolytes, *J. Phys. Chem. B* **111** (2007) 8369-8372.

47. Qiao, R., Ke, P.C., Lipid-carbon nanotube self-assembly in aqueous solution, *J. Am. Chem. Soc.* **128** (2006) 13656-13657.

48. Kharisov, B.I., Kharissova, O.V., Gutierrez, H.L., Méndez, U.O., Recent advances on the soluble carbon nanotubes, *Ind. Eng. Chem. Res.* **48** (2009) 572-590.

49. Coleman, J.N., Khan, U., Blau, W.J., Gun´ko, Y.K., Small but strong: a review of mechanical properties of carbon nanotube-polymer composites, *Carbon* **44** (2006) 1624–1652.

50. Blighe, F.M., Lyons, P.E., De, S., Blau, W.J., Coleman, J.N., On the factors controlling the mechanical properties of nanotube films, *Carbon* **46** (2008) 41–47.

51. Tchoul, M.N., Ford, W.T., Ha, M.L.P., Chavez-Sumarriva, I., Grady, B.P., Lolli, G., Resasco, D.E., Arepalli, S., Composites of single-walled carbon nanotubes and polystyrene: preparation and electrical conductivity, *Chem. Mater.* **20** (2008) 3120-3126.

52. Vesterinen, A., Rich, J., Seppälä, J., Synthesis and solution rheology of poly[(stearyl methacrylate)-stat-([2-(methacryloyloxy)ethyl] trimethyl ammonium iodide)], *J. Coll. Inter. Sci.* **351** (2010) 478–484.

53. Segui, C., Cesari, E., Pons, J., Chernenko, V., Internal friction behavior of Ni-Mn-Ga, *Mater. Sci. Eng. A* **370** (2004) 481-484.

54. Gans, E., Henry, C., Carman, G.P., High energy absorption in bulk ferromagnetic shape memory alloys ($Ni_{50}Mn_{29}Ga_{21}$). In *Smart Structures and Materials 2004: Active Materials: Behavior and Mechanics: 5387 (Proceedings of SPIE),* Edit. D.C. Lagoudas, SPIE, Bellingham 2004, pp. 177-185.

55. Chang, S.-H., Internal friction of Cu-13.5Al-4Ni shape memory alloy measured by dynamic mechanical analysis under isothermal conditions, *Mater. Lett.* **64** (2010) 93-95.

56. Raghavan, J., Bartkiewicz, T., Boyko, S., Kupriyanov, M., Rajapakse, N., Yu, B., Damping, tensile, and impact properties of superelastic shape memory alloy (SMA) fiber-reinforced polymer composites, *Compos. Part B* **41** (2010) 214-222.

57. Chang, S.-H., Low-frequency damping properties of near-stoichiometric Ni_2MnGa shape memory alloys under isothermal conditions, *Scripta Mater.* **59** (2008) 1039-1042.

58. Wang, W., Magnetically controlled high damping in ferromagnetic $Ni_{52}Mn_{24}Ga_{24}$ single crystal, *Appl. Phys. Lett.* **89** (2006) 101911-1-4.

59. López, G.A., Barrado, M., Juan, J.S., Nó, M.L., Cu-Al-Ni-SMA-based high-damping composites, *J. Mater. Eng. Perf.* **18** (2009) 459-462.

60. Ito, W., Imano, Y., Kainuma, R., Sutou, Y., Oikawa, K., Ishida, K., Martensitic and magnetic transformation behaviors in Heusler-type NiMnIn and NiCoMnIn metamagnetic shape memory alloys, *Metall. Mater. Trans. A* **38** (2007) 759-766.

61. Okamoto, N., Fukada, T., Kakeshita, T., Temperature dependence of martensite variants by magnetic field in 10M, 14M and 2M martensites of Ni-Mn-Ga alloys, *Mater. Sci. Eng. A* **481-482** (2008) 306-309.

62. Heczko, O., Straka, L., Temperature dependence and temperature limits of magnetic shape memory effect, *J. Appl. Phys.* **94** (2003) 7139-7143.

63. Neuking, K., Abu-Zafifa, A., Eggeler, G., Surface engineering of shape memory alloy/polymer-composites: Improvement of the adhesion between polymers and pseudoelastic shape memory alloys, *Mater. Sci. Eng. A* **481-484** (2008) 606-611.

64. Underhill, R.S., Stevens, K.A., Fisher, G.C., Surfactant modified nickel-manganese-gallium powder and silicone composites, *Adv. Sci. Techn.* **59** (2008) 35-40.

65. Underhill, R.S., Keddy, G.A., Farrell, S.P., Polymer assessment for magnetic shape memory alloy composites, *Proceedings of the MRS 2006 Fall Meeting,* Edit. L. Thilly, Material Research Society, Boston 2006, pp. 0977-FF13-01.

66. Conti, S., Lenz, M., Rumpf, M., Modeling and simulation of magnetic-shape-memory polymer composites, *J. Mech. Phys. Sol.* **55** (2007) 1462-1486.

67. Scheerbaum, N., Hinz, D., Gutfleisch, O., Müller, K.-H., Schultz, L., Textured polymer bonded composites with Ni-Mn-Ga magnetic shape memory particles, *Acta Mater.* **55** (2007) 2707-2713.

68. Rodriguez, C., Barrio, A., Orue, I., Vilas, J.L., Leon, L.M., Barandiaran, J.M., Frez-Gubieda Ruiz, M.L., High magnetostriction polymer-bonded Terfenol-D composites, *Sens. Actuators A* **142** (2008) 538-541.

69. Rodriguez, C., Rodriguez, M., Orue, I., Vilas, J.L., Barandiaran, J.M., Gubieda, M.L.F., Leon, L.M., New elastomer-Terfenol-D magnetostrictive composites, *Sens. Actuators A* **149** (2009) 251-254.

70. Tian, B., Chen, F., Tong, Y.X., Li, L., Zheng, Y.F., Liu, Y., The orientation dependence of transformation strain of Ni-Mn-Ga polycrystalline alloy and its composite with epoxy resin, *J. Alloys Compd.* **505** (2010) 680-684.

71. Feuchtwanger, J., Richard, M.L., Lazpita, P., Gutierrez, J., Barandiaran, J.M., Allen, S.M., O'Handley, R.C., Stress-induced twin boundary motion in particulate Ni-Mn-Ga/polymer composites, *Mater. Sci. Forum* **583** (2008) 197-212.

72. Bauhofer, W., Kovacs, J.Z., A review and analysis of electrical percolation in carbon nanotube polymer composites, *Compos. Sci. Technol.* **69** (2009) 1486–1498.

73. Grossiord, N., Loos, J., van Laake, L., Maugey, M., Zakri, C., Koning, C.E., Hart, A.J., High-conductivity polymer nanocomposites obtained by tailoring the characteristics of carbon nanotube fillers, *Adv. Funct. Mater.* **18** (2008) 3226-3234.

74. Bagchi, A., Nomura, S., On the effective thermal conductivity of carbon nanotube reinforced polymer composites, *Compos. Sci. Technol.* **66** (2006) 1703–1712.

75. Wunderlich, W., Physical constants of poly(methyl methacrylate), in *Polymer Handbook*, 4th Edition, Brandrup, J., Immergut, E.H., Grulke, E.A. (editors), John Wiley & Sons, USA **1999**, pp. V/87-V90.

76. van Herk, A.M. (Ed.), *Chemistry and technology of emulsion polymerization*, Blackwell Publishing Ltd., Oxford, Great Britain 2005, 307 p.

77. Krause, B., Mende, M., Pötschke, P., Petzold, G., Dispersability and particle size distribution of CNTs in an aqueous surfactant dispersion as a function of ultrasonic treatment time, *Carbon* **48** (2010) 2746-2754.

78. Blanch, A.J., Leneham, C.E., Quinton, J.S., Optimizing surfactant concentrations for dispersion of single-walled carbon nanotubes in aqueous solution, *J. Phys. Chem. B* **114** (2010) 9805-9811.

79. Rausch, J., Zhuang, R.-C., Mäder, E., Surfactant assisted dispersion of functionalized multi-walled carbon nanotubes in aqueous media, *Compos. Part A* **41** (2010) 1038-1046.

80. Yu, J., Grossiord, N., Koning, C.E., Loos, J., Controlling the dispersion of multi-walled carbon nanotubes in aqueous surfactant solution, *Carbon* **45** (2007) 618-623.

81. Yu, J., Lu, K., Sourty, E., Grossiord, N., Koning, C.E., Loos, J., Characterization of conductive multiwall carbon nanotube/polystyrene composites prepared by latex technology, *Carbon* **45** (2007) 2987-2903.

82. Angelikopoulos, P., Gromov, A., Leen, A., Nerushev, O., Bock, H., Campbell, E.E.B., Dispersing individual single-wall carbon nanotubes in aqueous surfactant solutions below the cmc, *J. Phys. Chem. C* **114** (2010) 2-9.

83. Cherkasova, A.S., Shan, J.W., Particle aspect-ratio and agglomeration-state effects on the effective thermal conductivity of aqueous suspensions of multiwalled carbon nanotubes, *J. Heat Trans.* **132** (2010) 082402.

84. He, G., Pan, Q., Synthesis of polystyrene and polystyrene/poly(methyl methacrylate) nanoparticles, *Macromol. Rapid Commun.* **25** (2004) 1545-1548.

85. Norakankorn, C., Pan, Q., Rempel, G.L., Kiatkamjornwong, S., Synthesis of poly(methyl methacrylate) nanoparticles initiated by 2,2´-azoisobutyronitrile via differential microemulsion polymerization, *Macromol. Rapid Commun.* **28** (2007) 1029-1033.

86. Tauer, K., Müller, H., On the role of initiator in emulsion polymerization, *Colloid Polym. Sci.* **281** (2003) 52-65.

87. Reddy, G.V.R., Devi, N.G., Panda, J., Microemulsion and conventional emulsion copolymerizations of styrene with methyl methacrylate, *J. Appl. Polym. Sci.* **105** (2007) 3391-3401.

88. Norakankorn, C., Pan, Q., Rempel, G.L., Kiatkamjornwong, S., Synthesis of poly(methyl methacrylate) nanoparticles initiated by azobisisobutyronitrile using a differential microemulsion polymerization technique, *J. Appl. Polym. Sci.* **113** (2009) 375-382.

89. Chen, W., Liu, X., Liu, Y., Bang, Y., Kim, H.-I., Synthesis of PMMA and PMMA/PS nanoparticles by microemulsion polymerization with a new vapor monomer feeding system, *Colloids Surf. A Physicochem. Eng. Asp.* **364** (2010) 145-150.

90. Aguilar, J., Rabelero, M., Nuño-Donlucas, S.M., Menzizábal, E., Martínez-Richa, A., López, R.G., Arellano, M., Puig, J.E., Narrow size-distribution poly(methyl methacrylate) nanoparticles made by semicontinuous heterophase polymerization, *J. Appl. Polym. Sci.* **119** (2011) 1827-1834.

91. Teo, B.M., Ashokkumar, M., Grieser, F., Microemulsion polymerizations via high-frequency ultrasound irradiation, *J. Phys. Chem. B Lett.* **112** (2008) 5265-5267.

92. Teo, B.M., Grieser, F., Ashokkumar, M., High intensity ultrasound initiated polymerization of butyl methacrylate in mini- and microemulsions, *Macromolecules* **42** (2009) 4479-4483.

93. Jiang, W., Yang, W., Zeng, X., Fu, S., Structure and properties of poly(methyl methacrylate) particles prepared by a modified microemulsion polymerization, *J. Polym. Sci. Part A: Polym. Chem.* **42** (2004) 733-741.

94. Jia, Z., Wang, Z., Xu, C., Liang, J., Wie, B., Wu, D., Zhu, S., Study on poly(methyl methacrylate)/carbon nanotube composites, *Mater. Sci. Eng. A.* **271** (1999) 395-400.

95. Park, S.J., Cho, M.S., Lim, S.T., Choi, H.J., Jhon, M.S., Synthesis and dispersion characteristics of multi-walled carbon nanotube composites with poly(methyl methacrylate) prepared by in-situ bulk polymerization, *Macromol. Rapid Commun.* **24** (2003) 1070–1073.

96. Xia, H., Qiu, G., Wang, Q., Polymer/carbon nanotube composite emulsion prepared through ultrasonically assisted in situ emulsion polymerization, *J. Appl. Polym. Sci.* **100** (2006) 3123-3130.

97. Wu, T.-M., Chen, E.-C., Preparation and characterization of conductive carbon nanotube-polystyrene nanocomposites using latex technology, *Compos. Sci. Technol.* **68** (2008) 2254–2259.

98. Morcom, M., Atkinson, K., Simon, G.P., The effect of carbon nanotube properties on the degree of dispersion and reinforcement of high density polyethylene, *Polymer* **51** (2010) 3540–3450.

99. McGlory, C., McNally, T., Baxendale, M., Pötchke, P., Blau, W., Ruether, M., Electrical and rheological percolation of PMMA/MWCNT Nanocomposites as a function of CNT geometry and functionality, *Eur. Polym. J.* **46** (2010) 854-868.

100. Sumfleth, J., Prehn, K., Wichmann, M.H.G., Wedekind, S., Schulte, K., A comparative study of the electrical and mechanical properties of epoxy nanocomposites reinforced by CVD- and arc-grown multi-wall nanotubes, *Compos. Sci. Tech.* **70** (2010) 173-180.

101. Kim, D.-Y., Yun, Y.S., Bak, H., Cho, S.Y., Jin, H.-J., Aspect ratio control of acid modified multiwalled carbon nanotubes, *Curr. Appl. Phys.* **10** (2010) 1046-1052.

102. Hermant, M.C., Smeets, N.M.B., van Hal, R.C.F., Meuldijk, J., Heuts, H.P.A., Klumperman; B., van Herk, A.M., Koning, C.E., Influence of the molecular weight distribution on the percolation threshold of carbon nanotube – polystyrene composites, *e-Polymers* (2009) 022.

103. Regev, O., ElKati, P.N.B., Loos, J., Koning, C.E., Preparation of conductive nanotube-polymer composites using latex technology, *Adv. Mater.* **16** (2004) 248-251.

104. Foygel, M., Morris, R.D., Anez, D., French, S., Sobolev, V.L., Theoretical and computational studies of carbon nanotube composites and suspensions: electrical and thermal conductivity, *Phys. Rev. B* **71** (2005) 104201.

105. Hecht, D., Hu, L., Grüner, G., Conductivity scaling with bundle lenght and diameter in single walled carbon nanotube networks, *Appl. Phys. Lett.* **89** (2006) 133112.

106. Li, C., Thostenson, E.T., Chou, T.-W., Dominant role of tunneling resistance in the electrical conductivity of carbon nanotube-based composites, *Appl. Phys. Lett.* **91** (2007) 223114.

107. Zhong, H., Lukes, J.R., Interfacial thermal resistance between carbon nanotubes: molecular dynamics simulations and analytical thermal modeling, *Phys. Rev. B* **74** (2006) 125403.

108. Gojny, F.H., Wichmann, M.H.G., Fiedler, B., Kinloch, I.A., Bauhofer, W., Windle, A.H., Schulte, K., Evaluation and identification of electrical and thermal conduction mechanisms in carbon nanotube/epoxy composites, *Polymer* **47** (2006) 2036–2045.

109. Cai, D., Song, M., Latex technology as a simple route to improve the thermal conductivity of a carbon nanotube/polymer composite, *Carbon* **46** (2008) 2107–2112.

110. Wang, G., Liu, Y., Self-assembly of carbon nanotubes modified by amphiphilic block polymers in selective solvent, *Macromol. Chem. Phys.* **210** (2009) 2070–2077.

111. Peponi, L., Valantini, L., Torre, L., Mondragon, I., Kenny, J.M., Surfactant assisted selective confinement of carbon nanotubes functionalized with octadecylamine in a poly(styrene-b-isoprene-b-styrene) block copolymer matrix, *Carbon* **47** (2009) 2474-2480.

112. Zou, J., Khondaker, S.I., Huo, Q., Zhai, L., A general strategy to disperse and functionalize carbon nanotubes using conjugated block copolymers, *Adv. Funct. Mater.* **19** (2009) 479–483.

113. Cho, J., Daniel, I.M., Dikin, D.A., Effects of block copolymer dispersant and nanotube length on reinforcement of carbon/epoxy composites, *Compos. Part A* **39** (2008) 1844–1850.

114. Cho, J., Daniel, I.M., Reinforcement of carbon/epoxy composites with multi-wall carbon nanotubes and dispersion enhancing block copolymers, *Scripta Mater*. **58** (2008) 533–536.

115. McClory, C., Pötschke, P., McNally, T., Influence on screw speed on electrical and rheological percolation of melt-mixed high-impact polystyrene/MWCNT nanocomposites, *Macromol. Mater. Eng*. **296** (2011) 59-69.

116. Socher, R., Krause, B., Boldt, R., Hermasch, S., Wursche, R., Pötschke, P., Melt mixed nano composites of PA12 with MWNTs: influence of MWNT and matrix properties on macrodispersion and electrical properties, *Compos. Sci. Tech*. **71** (2011) 306-314.

117. Zhou, Z., Wang, S., Lu, L., Zhang, Y., Zhang, Y., Preparation and rheological characterization of poly(methyl methacrylate)/functionalized multi-walled carbon nanotubes composites, *Compos. Sci. Tech*. **67** (2007) 1861-1869.

118. Prashantha, K., Soulestin, J., Lacrampe, M.F., Krawczak, P., Dupin, G., Claes, M., Masterbatch-based multi-walled carbon nanotubes filled polypropylene nanocomposites: assessment of rheological and mechanical properties, *Compos. Sci. Tech*. **69** (2009) 1756-1763.

119. Prashantha, K., Soulestin, J., Lacrampe, M.F., Claes, M., Dupin, G., Krawczak, P., Multi-walled carbon nanotube filled polypropylene nanocomposites based on masterbatch route: improvement of dispersion and mechanical properties through PP-g-MA addition, *eXPRESS Polym. Lett*. **2** (2008) 735-745.

120. Pötschke, P., Bhattacharyya, A.R., Janke, A., Carbon nanotube-filled polycarbonate composites produced by melt mixing and their use in blends with polyethylene, *Carbon* **42** (2004) 965-969.

121. Li, Y., Shimizu, H., Conductive PVDF/PA6/CNTs nanocomposites fabricated by dual formation of cocontinuous and nanodispersion structures, *Macromolecules* **41** (2008) 5339-5344.

122. Pan, Y., Li, L., Chan, S.H., Zhao, J., Correlation between dispersion state and electrical conductivity of MWCNTs/PP composites prepared by melt blending, *Compos. Part A* **41** (2010) 419-426.

Aalto-DD 126/2011

ISBN 978-952-60-4387-6
ISBN 978-952-60-4388-3 (pdf)
ISSN-L 1799-4934
ISSN 1799-4934
ISSN 1799-4942 (pdf)

Aalto University
School of Chemical Technology
Department of Biotechnology and Chemical Technology
www.aalto.fi

BUSINESS + ECONOMY

ART + DESIGN + ARCHITECTURE

SCIENCE + TECHNOLOGY

CROSSOVER

DOCTORAL DISSERTATIONS